

R&D of gas filled detectors for High Energy Physics experiments

Saikat Biswas¹

¹*Department of Physics and Centre for Astroparticle Physics and Space Science (CAPSS), Bose Institute, EN-80, Sector V, Kolkata-700091, India*

July 4, 2021

Abstract

BOSE Institute is Asia's first modern research centre devoted to interdisciplinary research and bears a century old tradition of research excellence. In the Experimental High Energy Physics (EHEP) detector laboratory of Bose Institute, Kolkata, we are working on the R&D of Gas Electron Multiplier (GEM), straw tube detector for future heavy ion physics experiments and also developing low resistive bakelite Resistive Plate Chamber (RPC), keeping in mind high particle rate handling capacity. The main goal of our research program is the stability study and ageing study of gaseous detectors mentioned above. In this review article, the details of the R&D program of GEM detector, straw tube and RPC detectors carried out during the last five years is reported.

1 Introduction

The advent of high-rate experiments, e.g. HERA-B at DESY and more recently experiments at the CERN LHC, requires innovative detector concepts. Micro Pattern Gas Detectors (MPGD) have become a promising route for handling high rates over the past two decades. The invention of MPGDs, in particular, the Gas Electron Multiplier (GEM) [1] or the Micro-Mesh Gaseous Structure (Micromegas) [2], and more recently other micro pattern detectors, offers the potential of gas detectors with very good spatial resolution, high rate handling capability, large sensitive area, stability of operation and radiation hardness [3]. These detectors can also achieve reasonably good energy and time resolution. Modern photo-lithographic technology has enabled a series of inventions revolutionising the cell size limits for many gas detector applications.

Several High Energy Physics (HEP) Experiments are already making use of this technology. Triple GEMs have been demonstrated to operate for over ten years in the COMPASS experiment [4] in a relatively high rate environment as tracking detectors. Future experiments, e.g. the Compressed Baryonic Matter (CBM) experiment at the future Facility for Antiproton and Ion Research (FAIR) in Darmstadt, Germany, will use triple GEM detectors to instrument the muon detector MUCH (MUon Chamber) [5, 6, 7, 8, 9, 10, 11, 12, 13]. 1st and 2nd stations of CBM-MUCH will use large-sized triple GEM detectors, where a high rate of particle flux is expected. A Large Ion Collider Experiment (ALICE) at the Large Hadron Collider (LHC) facility at CERN is upgrading the multi-wire proportional chamber based Time Projection Chamber (TPC) with quad GEM units, to cope up with the foreseen increase of the LHC luminosity in Pb-Pb collisions after Long Shutdown 2 (LS₂) [14, 15]. In order to achieve a low ion backflow ($< 1\%$) and good energy resolution (better than 28% (FWHM) for Fe⁵⁵ X-rays), it is decided that the new read-out chambers will consist of stacks of 4-GEM foils combining different hole pitches. However, the size of standard GEMs is, for technological reasons, limited to a size below $40 \times 40 \text{ cm}^2$. To minimize dead space in large area experiments, it is highly desirable to have larger-area gas detectors ($> 0.2 \text{ m}^2$) at hand. A potential candidate is GEMs, fabricated in a newly developed single mask technology [16].

In line with the worldwide efforts, in the EHEP detector laboratory of Bose Institute, Kolkata, we have also taken the initiative to carry on research and development with GEM detector prototypes. The main emphasis of this research program is the long-term stability study of GEM detector. In this work both single mask and double mask GEM detectors are used. For both the chambers, the GEM foils and other components of the detectors are obtained from CERN [17] and also assembled in the RD51 laboratory of CERN [18]. The details of the R&D activities on GEM detectors are described in Sec. 2.

On the other hand, several kinds of wire chambers are still used for particle tracking, but ageing problems result in a more pronounced non-linearity of the space-time correlation and a moderate loss in position accuracy. However, the space-time correlation is affected by the counting rate due to the accumulation of positive ions and the resulting space-charge field distortion. A limitation for using the drift tubes lies in the thickness of the cathodes; acceptable for high-energy muon detection, it causes a deterioration of tracking accuracy for lower momentum particles. The development of techniques capable of manufacturing single-wire counters with thin plastic walls, the so-called straws, permits the realisation of large arrays of light detectors. Straw drift chambers are used for the Large Area Tracking (LAT) of the Common Muon and Proton Apparatus for Structure and Spectroscopy (COMPASS) at CERN [19].

Straw tubes are currently being used in large HEP experiments such as ATLAS [20] and NA62 [21] experiments at CERN and GlueX [22] in Hall D at JLab, as tracking detector with a low material budget [23, 24]. A straw tube detector is basically a gas filled single channel drift tube with a conductive inner layer as the cathode and a wire stretched along the axis as the anode. When high voltage is applied between the wire and the tube an electric field is generated in the gas filled region. The electric field separates electrons and positive ions produced by an incident charged particle along its trajectory through the gas volume. The wire is kept at a positive voltage and collects the electrons while the ions drift towards the cathode. By choosing thin wires, with a diameter of a few tens of μm , the electric field strength near the wire is made high enough to create an avalanche of electrons. Depending on the high voltage and the gas composition, a gain of about $10^4 - 10^5$ can be achieved [25]. The specific energy loss (dE/dx) of a charged particle in the gas volume of the straw tube can be used to identify the particle species and can be derived from the number of ionisation electrons per track length (dx) for the generated straw signal. The main advantage of using straw tube in a tracking system is the reduction of material budget. Straw tube detectors are one of the options for the 3rd and 4th stations of CBM-MUCH.

Another large area gaseous detector called the Resistive Plate Chambers (RPCs), first developed by Santonico et al. [26, 27, 28, 29] using bakelite are used extensively in HEP experiments. The RPCs are being considered for the following reasons a) relatively low cost of materials used in making RPCs, b) robust fabrication procedure and handling and c) excellent time and position resolution. Primarily used for generating fast trigger for muon detection [30], time of flight (TOF) [31, 32] measurement, and tracking capabilities in multi layer configurations, they are successfully used in BELLE [33], BaBar [34], BESIII [35], and several LHC experiments (ATLAS, CMS etc.) [36, 37]. RPCs are used in neutrino experiments like OPERA, where its excellent time resolution and tracking capabilities are exploited [38]. The RPCs are also being explored for use in the Positron Emission Tomography (PET) imaging with TOF-PET [39], detection of γ -rays [40] and neutrons [41, 42] over a large area.

The RPCs are made up of high resistive (bulk resistivity $\sim 10^{10}$ - 10^{11} Ω cm) plates (e.g. glass, bakelite) as electrodes, which help to contain the discharge created by the passage of a charged particle or by an ionising radiation in a gas volume, and pick-up strips are used to collect the resulting signals. The typical time resolution for a single gap RPC is ~ 1 -2 ns. By reducing the gaps between the electrodes or by using multi-gap configuration, time resolution in such a detector can be improved to < 100 ps [43, 44]. The position resolution of RPCs is 1 cm to ~ 100 μm .

The RPCs are operated in two modes, viz., the avalanche mode and the streamer mode. Over the years, one of the main concerns with the use of RPCs is their long-term stability. In the avalanche mode, a small amount of charge (~ 1 pC) is produced in the gas, which allows the RPC to recover in a relatively shorter time to handle high counting rates (~ 1 kHz/cm²). Ageing effects caused by the accumulated charge is also relatively less in this mode. In the streamer mode of operation, the amount of charge produced after ionisation is considerably larger, creating induced signals of larger magnitude. But, the recovery time is also larger and the irreversible damage caused by the accumulated charge reduces the life of the RPC. However, several remedial measures can be taken to prolong its life under the streamer mode of operation. Careful choice of materials, smoothness of the surfaces to avoid localisation of excess charges, surface treatment to reduce the surface resistivity or providing alternate leakage path for post-streamer recovery are adopted in the major high energy physics experiments. Prolonged stable operation in streamer mode of the BELLE RPCs, though made of glass, is a testimony to many serious efforts taken for the above cause [33, 45].

RPCs are generally used for moderate rate handling (~ 1 -5 kHz/cm²). In our research project, we propose a systematic investigation of RPC for intermediate rate operations (~ 10 -15 kHz/cm²). We plan to investigate RPCs employing an X-ray generator and cosmic rays in the laboratory as well as charged particle beams and in particular hadronic beams and hadronic showers, delivered by the CERN SPS. There is foreseen to test RPCs in a harsh hadronic environment similar to the CBM experiment, particularly after the hadron absorber. In

this regard RPCs are another option for the 3rd and 4th stations of CBM-MUCH.

In the last two decades, India is progressing well in the field of research on gaseous detectors. The gaseous Photon Multiplicity Detector (PMD) developed in India is being successfully used in the STAR experiment at Relativistic Heavy Ion Collider (RHIC) in BNL and A Large Ion Collider Experiment (ALICE) at CERN in LHC [46, 47].

Apart from this, lots of R&D on RPC are being carried out both using glass and bakelite for the future India-based Neutrino Observatory (INO) [48, 49, 50, 51, 52, 53, 54]. Starting from a 30 cm × 30 cm bakelite RPC obtained from China, a number of RPCs are developed, making use of the bakelite plates available locally in India. The entire effort can be divided into the following steps: (a) Characterization of different grades of bakelite in terms of resistivity (bulk and surface) and other electrical properties and thereby choosing the electrically suitable bakelite for RPC-building (b) Building of RPCs (10 cm × 10 cm and 30 cm × 30 cm), detailed procedure involved building of the components like button and edge spacers, gas nozzles, pick-up strips, graphite coating arrangement by adjusting the resistivity, connection of high voltage leads (c) Testing of the RPCs in a cosmic ray stand by measuring the efficiency, count rate, time resolution and long-term stability in the streamer mode of operation (d) To improve the performance of the detector, a thin layer of silicone coating is applied to the inner surfaces of the electrodes towards maintaining the surface smoothness. One such silicone coated RPC is tested for a long duration showing ~ 96% efficiency for a period of operation of more than 130 days. The time resolution measured for the RPCs reaches ~ 2 ns and the measured charge content is ~ 100 pC at a high voltage of 8 kV. Consistency of results is established by making several such RPC modules. Operating the detectors in the avalanche mode and studying the properties like efficiency, time resolution, charge content in the various composition of gases are also used for further study and finally, building of the 1m × 1m RPC is completed for use in a prototype calorimeter. The work started from scratch and at the end, silicone-coated bakelite-based RPCs even working in streamer mode are established as an alternative to glass-based RPC working in avalanche mode. Apart from being less expensive, larger pulses and fewer electronic components in the streamer mode of operation make bakelite-based RPCs even more attractive. All the activities are part of the R&D effort towards building ICAL detector in INO. In this context, the development and satisfactory performance of bakelite-based RPCs open up a new avenue for the sensitive detectors in ICAL. ICAL requires about 27000 large size RPC modules and there is always a possibility of using more than one type of electrode materials. Bakelite-based RPCs are attractive from the point of view that the materials are locally made. This work is likely to open up the horizon for the active detectors for ICAL.

Indian researchers are working on the use of gas filled detector such as Multigap Resistive Plate Chamber (MRPC) for medical imaging in place of the expensive scintillator detector [55].

Presently, dedicated R&D is in progress on the GEM based detectors for the CBM Muon Chamber detector at FAIR and for the upgrade of ALICE Time Projection Chamber.

This particular review article is based on the R&D activities done in the EHEP detector laboratory of Bose Institute, Kolkata on GEM detector, Straw tube detector and bakelite RPC [56, 57, 58, 59, 60, 61, 62].

2 GEM detectors

2.1 Description of the GEM detector prototypes and electronics setup

In this work, both single mask and double mask triple GEM detector prototypes are used. In this article, the single mask and double mask triple GEM detector prototypes will be named as SM and DM respectively. Both the GEM detector prototypes, consisting of 10 cm × 10 cm standard stretched foils, obtained from CERN are assembled in the clean room of the RD51 laboratory [18]. The drift gap, transfer gap 1, transfer gap 2 and the induction gap of both the chambers are kept as 3, 2, 2, 2 mm respectively. In case of SM, although a triple GEM detector is built, there is a provision of adding one more GEM foil to make it a quadrupole chamber prototype [15]. To keep this provision, two G10 edge frames of thickness 10 mm are used to make the gas enclosure. In such a system, the Kapton window is eventually placed 11 mm above the drift plane. A voltage divider chain is also built by resistors and a single negative high voltage (HV) channel is used to power the chamber. The chamber has an XY printed board (256 X-tracks, 256 Y-tracks) on the base plate and that works as the readout plane. Each of 256 X-tracks and 256 Y-tracks is connected to two 128 pin connectors. In each 128 pin connector, a sum-up board (provided by CERN) is used. Total 4 sum-up boards are used in this prototype. The Lemo output of the 4 sum-up boards are again summed and is directly connected by a short length Lemo cable to a 6485 Keithley Pico-ammeter to measure the total anode current [56].

In case of DM prototype also the HV to the drift plane and individual GEM planes are applied through a

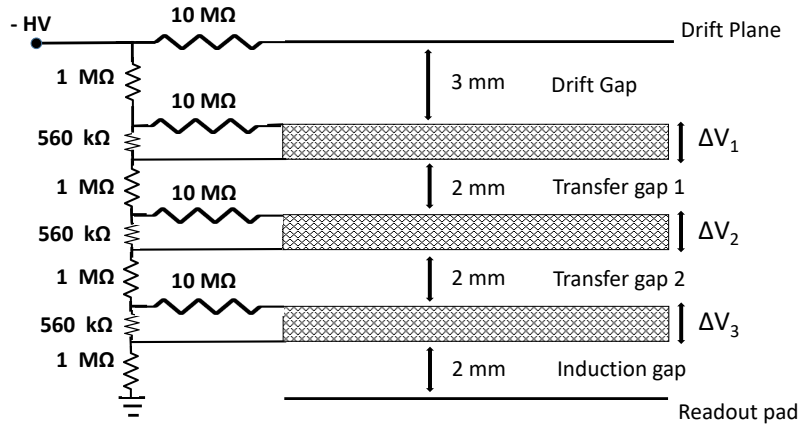


Figure 1: Schematic of the HV distribution of the double mask triple GEM chamber. The drift gap, transfer gap and induction gaps are kept at 3 mm, 2 mm, and 2 mm respectively.

voltage dividing resistor network. $10\text{ M}\Omega$ protection resistors are used to the drift plane and top of each GEM foil. A schematic of the resistor chain and different gaps of the chamber is shown in Figure 1. In this case also, although there are segmented readout pads each of dimension $9\text{ mm} \times 9\text{ mm}$, the signals are collected from all the pads added by a sum-up board and a single input is fed to a charge sensitive preamplifier (VV50-2) [64]. The gain of the charge sensitive preamplifier is 2 mV/fC and the shaping time is 300 ns. A NIM based data acquisition system is used after the preamplifier. The same signal from the preamplifier is used to measure the rate and to obtain the energy spectrum. For this purpose, the output signal from the preamplifier is fed to a linear Fan-in-Fan-out (linear FIFO) module for this purpose. The analog signal from the linear FIFO is put to a Single Channel Analyser (SCA) to measure the rate of the incident particle. The SCA is operated in integral mode and the lower level in the SCA is used as the threshold to the signal. The threshold in SCA is set at 0.1 V to reject the noise. 0.1 V corresponds to 3σ of the typical noise level. At a typical HV of - 4150 V with 0.1 V threshold, the noise rate is found to be 45 Hz. The discriminated signal from the SCA, which is TTL in nature, is fed to a TTL-NIM adapter module and the output NIM signal is counted using a NIM scaler. The count rate of the chamber in Hz is then calculated. Another output of the linear FIFO module is put to a Multi Channel Analyser (MCA) to obtain the energy spectrum. A schematic representation of the set-up is shown in Figure 2 [57, 58, 59].

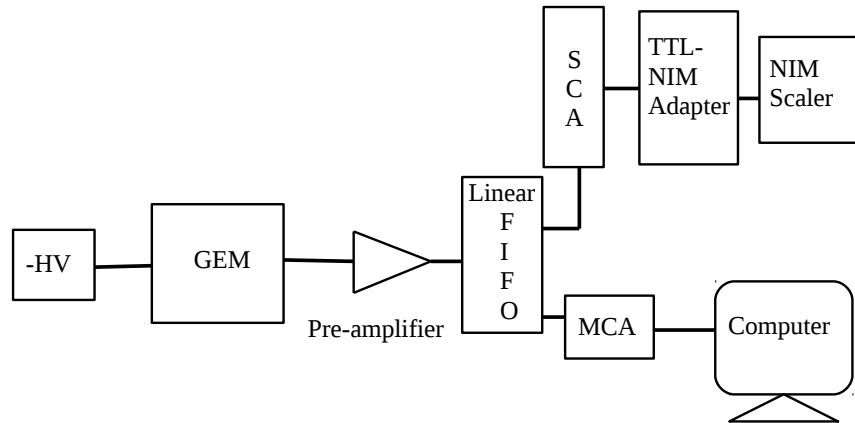


Figure 2: Schematic representation of the electronics setup.

For both the detectors, a pre-mixed Ar/CO₂ gas in 70/30 volume ratio is used for the stability study. A constant gas flow rate of 3 l/h is maintained using a Vögtlin gas flow meter, obtained from CERN. For the DM

chamber, Ar/CO₂ in 80/20 and 90/10 are also used. All the other details of the experiment and the results are described in Section 2.2.

2.2 Experiment details and Results

One of the important parameters for the GEM detectors to be used in recent HEP experiments is the long-term stability of the gain of the detector. In that spirit, the following studies are performed for both the SM and DM GEM detector prototypes. For the SM chamber, the stability test is performed measuring the anode current whereas that for the DM prototype is done from the spectra. In both the measurements, a strong Fe⁵⁵ X-ray source (activity 3.7 GBq) is used.

2.2.1 Long-term test of the single mask GEM detector

During the long-term test of the SM chamber, a constant HV of -4300 V is applied to the drift plane. The current through the voltage divider chain is measured from the HV power supply module. From the measured current and the known resistance value, the voltages across the GEM foils and that across the different gaps are calculated. At an applied voltage of -4300 V, the typical electric fields in the drift, transfer and induction gaps are found to be ~ 2.4 kV/cm, 3.6 kV/cm and 3.6 kV/cm respectively and the voltage differences across the three GEM foils from top to bottom i.e. ΔV_1 , ΔV_2 and ΔV_3 are ~ 395 V, 360 V and 320 V respectively. A mechanical jig is built to keep the Fe⁵⁵ X-ray source on top of the detector. A place on the detector is marked to keep the source and to ensure that the source always irradiates a particular area of the detector. The collimator on the jig is made exactly the same as the area of the source window. The source window diameter is 7.3 mm. The details of the jig and mechanical structure of the detector are shown in Figure 3 [56].

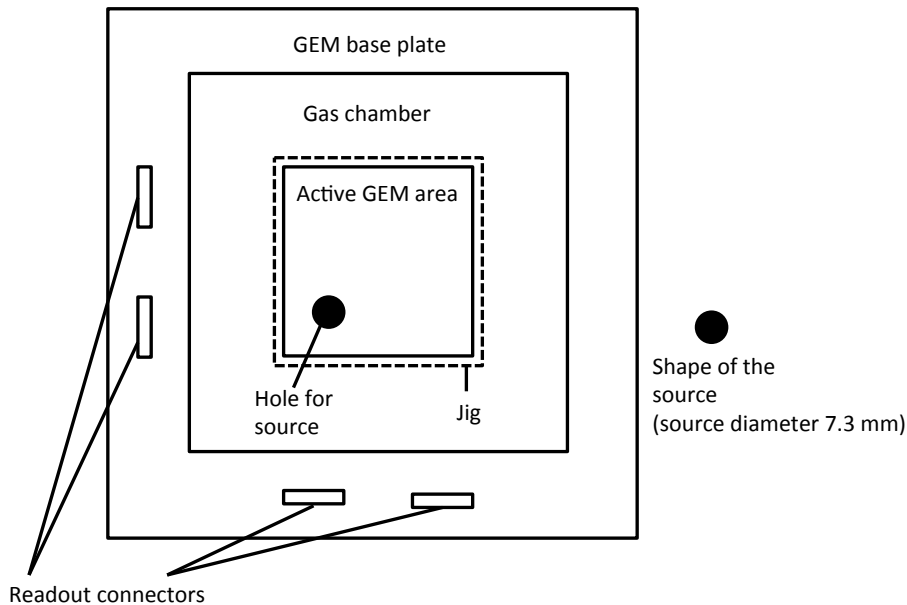


Figure 3: Schematic of the GEM chamber. The dimension of the GEM base plate is 25 cm \times 25 cm. The area of the gas sealed chamber is 20 cm \times 20 cm. The central active area of the GEM is 10 cm \times 10 cm. The jig (marked as a dotted square) is of area 10.5 cm \times 10.5 cm and its position just on top of the active GEM area is marked. A hole is made on the jig. The diameter of the hole is exactly the same as the diameter of the Fe⁵⁵ source. The source is circular in shape. The diameter of the source window is 7.3 mm (also shown in the figure).

The HV to the GEM chamber is increased and the signals from the readout plane are counted for a fixed time interval. For all voltage settings, the signals are counted from a scaler counter with a Fe⁵⁵ X-ray source

and also for the background. The background count is subtracted from the count with Fe^{55} source to get the count rate due to the source only for each voltage setting. The count rate is found to increase with the increase of HV and reaches a plateau. At plateau, the count rate is found to be ~ 350 kHz [56].

The stability of the gain for the chamber is studied using a Fe^{55} X-ray source and measuring the anode current with and without the source continuously [65, 66]. Similar type of measurements were also carried out previously using an 8 keV Cu X-ray generator and Sr^{90} beta radioactive source as referred in [65] and [66] respectively. At an interval of 15 minutes, the anode current with and without the source is measured. Actually, the source is kept on the particular position of the GEM detector for continuous irradiation and at an interval of 15 minutes the anode current is recorded, then the source is removed and the background current without the source is also recorded. Immediately after that, the source is placed in the same position again for the irradiation. Simultaneously the ambient temperature (t in $^{\circ}\text{C}$), atmospheric pressure (p in mbar) and relative humidity (RH in %) are also recorded using a data logger, built in-house, with a time stamp [67, 68]. The variation of the anode current with and without the radioactive source as a function of time is shown in Figure 4.

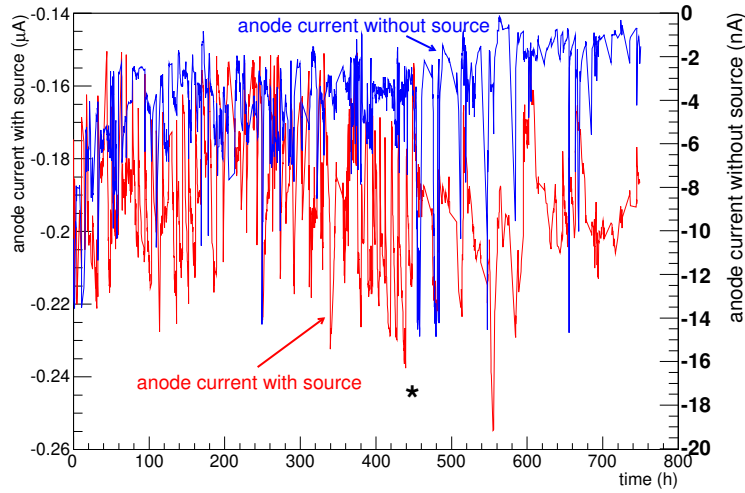


Figure 4: The anode current with Fe^{55} source and without the source as a function of time. The star (*) mark indicates an exchange of the gas cylinder. With Ar/CO_2 in the 70/30 volume ratio.

The output anode current due to the source only is given by,

$$i_{source} = i_{with\ source} - i_{without\ source} \quad (1)$$

where i_{source} is the anode current due to the radioactive source, $i_{with\ source}$ is the measured anode current when the detector is irradiated by the Fe^{55} source and $i_{without\ source}$ is the anode current without any source i.e. the background.

The gain of the detector is then calculated using the relation

$$gain = \frac{i_{source}}{r \times n \times e} \quad (2)$$

where, r is the rate of the incident X-rays, n is the number of primary electrons produced after full absorption of 5.9 keV Fe^{55} X-ray and e is the electronic charge. For each 5.9 keV Fe^{55} X-ray photon fully absorbed in Ar/CO_2 gas in 70/30 volume ratio n is 212. Since in this measurement, a Fe^{55} X-ray source is used and this source has a finite half life of ~ 2.7 years, the rate of the X-ray in the above equation is modified according to the relation:

$$r = r_0 \exp\left(\frac{-0.693 t'}{t_{1/2}}\right) \quad (3)$$

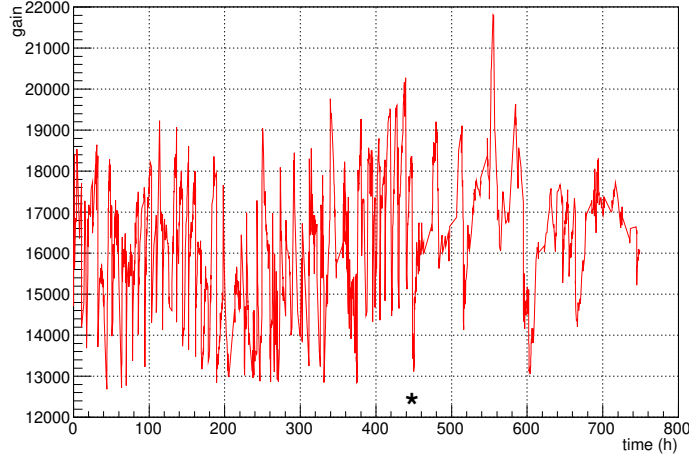


Figure 5: Measured gain as a function of time. The star (*) mark indicates an exchange of the gas cylinder. With Ar/CO₂ in the 70/30 volume ratio.

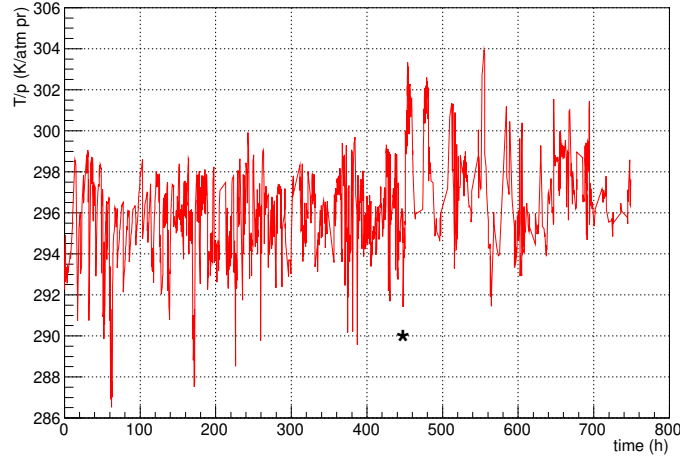


Figure 6: T/p as a function of the time. The star (*) mark indicates an exchange of the gas cylinder.

r_0 being 350 kHz, t' is the period of operation and $t_{1/2}$ is the half life of the Fe⁵⁵ source. Measured gain as a function of the total period of operation is shown in Figure 5. It is well known that the gain of any gaseous detector depends significantly on T/p. The ratio T/p during that time as a function of the total period of operation is shown in Figure 6, where T ($= t+273$) is the absolute temperature in Kelvin and p (p in mbar/1013) is in atmospheric pressure. The dependence of the gain (G) of a GEM detector on absolute temperature and pressure is given by [70]

$$G(T/p) = Ae^{(B\frac{T}{p})} \quad (4)$$

where A and B are the parameters to be determined from the correlation plot.

The correlation plot, i.e. the gain is drawn as a function of T/p and fitted with a function

$$gain(T/p) = Ae^{(B\frac{T}{p})} \quad (5)$$

is shown in Figure 7.

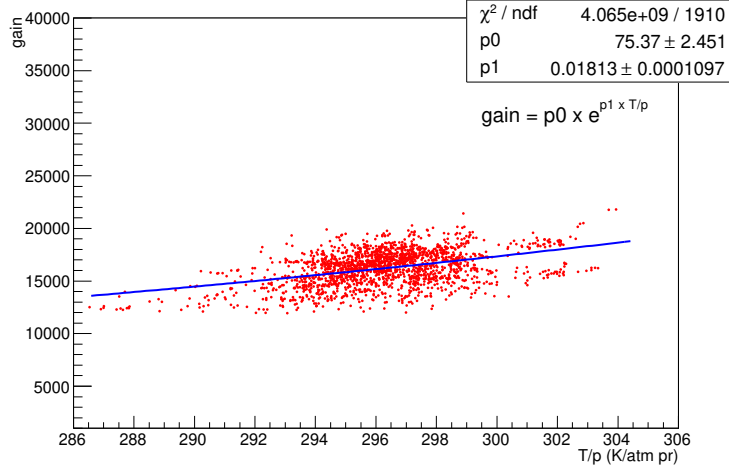


Figure 7: Correlation plot: Variation of the gain as a function of T/p . With Ar/CO₂ in the 70/30 volume ratio.

The values of the fit parameters A and B are found to be 75.37 ± 2.451 and 0.0181 ± 0.0001 atm pr/K. Using the fit parameters, the measured gain is normalized by using the formula:

$$gain_{normalized} = \frac{gain_{measured}}{Ae^{(B\frac{T}{p})}} \quad (6)$$

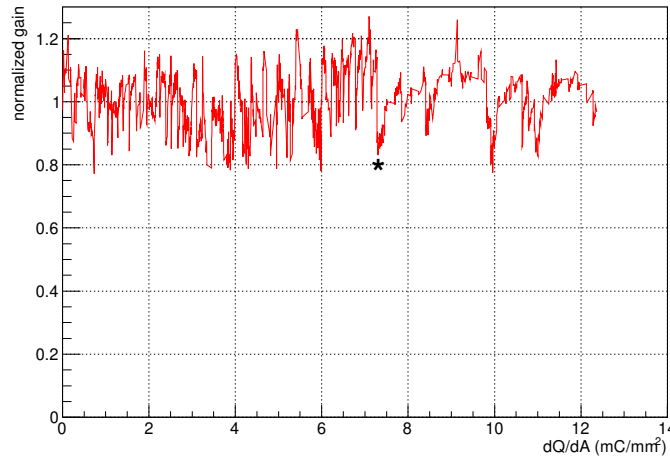


Figure 8: Normalized gain as a function of charge per unit area i.e. dQ/dA . The star (*) mark indicates an exchange of the gas cylinder. With Ar/CO₂ in the 70/30 volume ratio.

To check the stability of the detector with continuous radiation, the variation of the normalized gain is drawn as a function of the total charge accumulated per unit irradiated area of the detector, i.e. dQ/dA (that is directly proportional to time). To calculate the total charge accumulated, the average anode current $(i_1 + i_2)/2$ of two time, say t_1 and t_2 is taken and multiplied by the time interval $(t_2 - t_1)$. The total charge accumulated will be the sum of the accumulated charge over all the intervals during every two adjacent readings. To get the total accumulated charge per unit area, the total accumulated charge is divided by the irradiated area. So mathematically the total charge per unit area is given by $\sum[\frac{(i_j + i_{j+1})}{2}(t_{j+1} - t_j)]/A$. Where A is the irradiated area. The normalized gain as a function of dQ/dA is shown in Figure 8. The distribution of the normalized gain fitted with a Gaussian function is shown in Figure 9. The mean of the distribution is found to be around

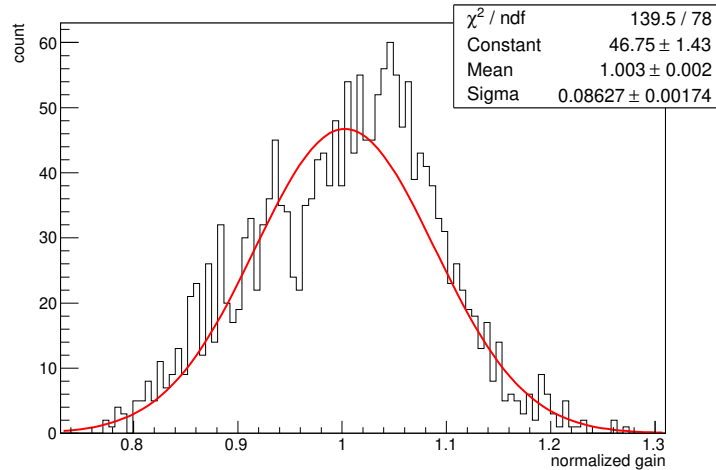


Figure 9: The distribution of the normalized gain fitted with a Gaussian function. With Ar/CO₂ in the 70/30 volume ratio.

1.003 with a sigma of 0.086 as shown in Figure 9. The T/p corrections do not reduce the spread in gain very much. The left-over spread, shown in Figure 9, is significantly large with respect to the variation due to the varying T/p. Although there is a fluctuation about the mean value of 1.003 in the normalized gain in Figure 8, there is no steady reduction in the normalized gain. Ageing is not observed even after operation of the GEM chamber for about 450 hours or after an accumulation of charge per unit area $\sim 7.25 \text{ mC/mm}^2$. After that, the old gas cylinder is replaced with a new one of the same mixture. This discontinuity is marked with a star (*) in Figures 4, 5, 6 and 8. With the new cylinder also there is no decrease in the normalized gain other than a fluctuation. It is to be mentioned here that because of intrinsic gain inhomogeneities for GEM geometry variations and also for the inhomogeneity in the gap between the individual GEM foils a gain variation up to 25% is possible which is extremely well described in References [71, 72]. (However, in the experimental method described here, the source irradiates a particular region of the detector and the total summed anode current is measured to calculate the gain as stated in Section 2.1. So the intrinsic gain variation will not affect the result.) In this study, we have arrived at a conclusion that no ageing is observed till the accumulation of charge per unit area $> 12.0 \text{ mC/mm}^2$ [56]. However, in this experiment, we have only monitored the gain of the detector and investigated its stability under continuous radiation. From the perspective of high energy physics experiment where GEMs will be used as tracking devices, the detector's energy resolution is also a parameter of concern. In that direction the next experiment is performed where we have monitored both the gain and energy resolution of a double mask GEM.

2.2.2 Long-term test of the double mask GEM detector

The stability test of the DM detector with Ar/CO₂ in 70/30 ratio is carried out at an applied HV of - 4100 V corresponding to a $\Delta V \sim 383.7 \text{ V}$ across each GEM foil, using the same Fe⁵⁵ X-ray source. The current through the divider chain is found to be $\sim 694 \mu\text{A}$. The drift, transfer and induction fields are kept constant at 2.3 kV/cm, 3.4 kV/cm and 3.4 kV/cm respectively. In this case, a particular circular patch of the detector is exposed to X-rays from a Fe⁵⁵ source. A G-10 collimator of diameter 8 mm is used to confine the X-rays to a circular patch of $\sim 50 \text{ mm}^2$ of the GEM detector.

In this study also, at first the bias voltage to the detector is increased and the count rate is measured to get the exposure rate. It is observed that as the efficiency of the detector increases with the increase of voltage so does the count rate and a plateau is observed from ΔV of 378.7 V onwards. ΔV across the top and bottom of the GEM foil is kept the same for all three GEM planes. The count rate as a function of the ΔV is shown in Figure 10. The saturated value of the count rate has been found to be $\sim 350 \text{ kHz}$, which is also the rate at which the stability test is performed. This value of the X-ray rate is used to calculate the accumulated charge later in this section.

The gain and the energy resolution of the chamber are measured from the energy spectra for the Fe⁵⁵ X-ray

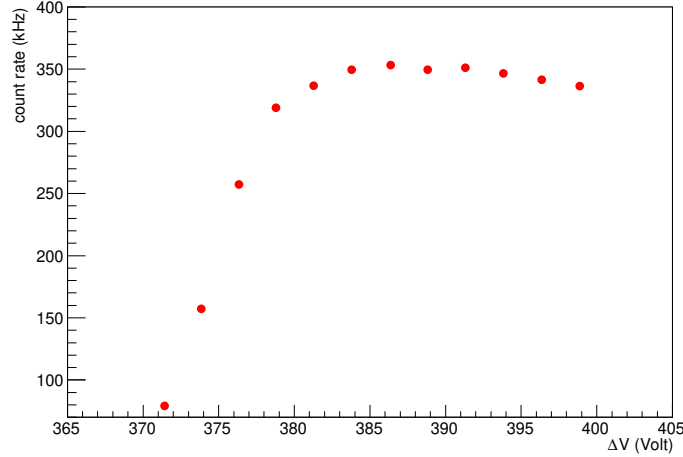


Figure 10: Count rate as a function of ΔV across each GEM foil. With Ar/CO₂ in the 70/30 volume ratio.

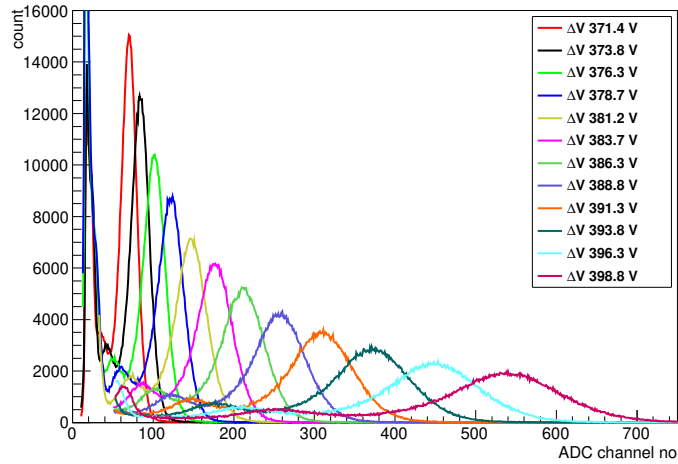


Figure 11: Energy spectra of the GEM detector at different ΔV . With Ar/CO₂ in the 70/30 volume ratio.

source. Typical energy spectra recorded with Fe⁵⁵ source at different ΔV are shown in Figure 11. For all the voltage settings the main peak (5.9 keV full energy peak) and the Argon escape peak are clearly visible along with the noise peak at the extreme left.

The expression for the gain is given by:

$$gain = \frac{\text{output charge}}{\text{input charge}} \quad (7)$$

$$= \frac{(\text{mean pulse height}/2\text{mV}) \text{ fC} \times 10^{15}}{\text{No. of primary electrons} \times e C} \quad (8)$$

where the mean pulse height for 5.9 keV peak of Fe⁵⁵ X-ray spectrum in ADC channel number is obtained by Gaussian fitting and that in mV is obtained from the ADC calibration curve (ADC channel no. vs pulse height). The preamplifier used in the set-up offers a gain of 2 mV/fC which is used in the expression for gain. The input charge is the primary number of electrons produced in the gas volume of the detector as a result of the total absorption of an 5.9 keV X-ray photon, multiplied by the electronic charge (e). For gain calculation, the average number of primary electrons for each Fe⁵⁵ X-ray photon of energy 5.9 keV, fully absorbed in the 3 mm

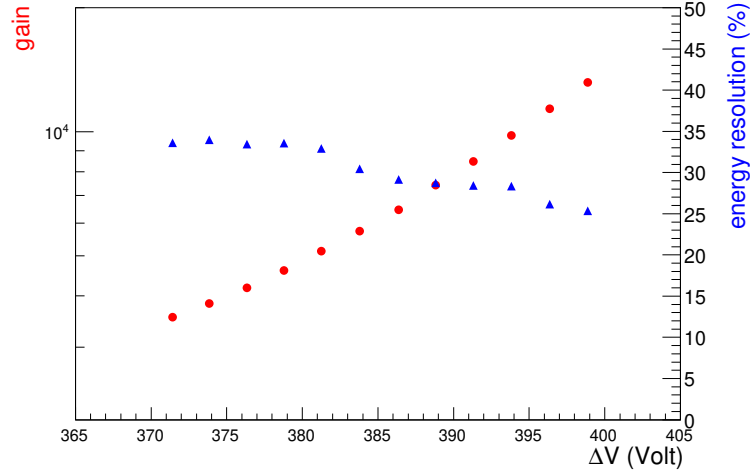


Figure 12: The gain and the energy resolution as a function of ΔV . The error bars are smaller than the symbols. With Ar/CO₂ in the 70/30 volume ratio.

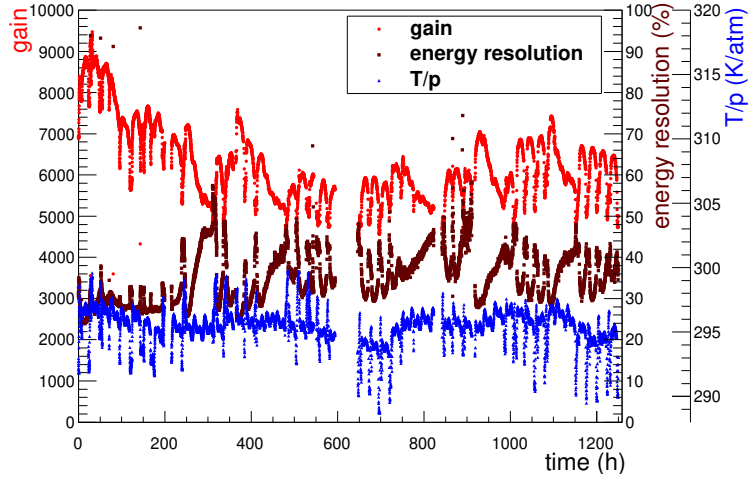


Figure 13: Variation of the measured gain, energy resolution and T/p as a function of time. The error bars are smaller than the symbols for gain. With Ar/CO₂ in the 70/30 volume ratio.

drift gap in Ar/CO₂ gas with 70/30 volume ratio is taken as 212 whereas that in 80/20 and 90/10 mixture are 217 and 222 respectively.

The energy resolution of the detector is defined as:

$$\% \text{ energy resolution} = \frac{\sigma \times 2.355}{\text{mean}} \times 100\% \quad (9)$$

where the sigma and the mean are obtained from the Gaussian fitting of the energy spectra. It is well known that the energy resolution improves with a decreasing value. The gain and energy resolution are measured by increasing the ΔV i.e. increasing the biasing voltage of the GEM detector. Both the gain and the energy resolution as a function of ΔV across a GEM foil are shown in Figure 12. It is observed that the gain of the detector increases exponentially from a value of ~ 3500 to 14000, whereas the energy resolution value decreases from 34% to 25% (FWHM) for a ΔV of 370 V to 400 V respectively.

For the stability study of the DM chamber, the same Fe⁵⁵ X-ray source is used to irradiate the detector as well as to obtain the spectrum. The circular area of $\sim 50 \text{ mm}^2$ of the GEM detector is exposed from the top

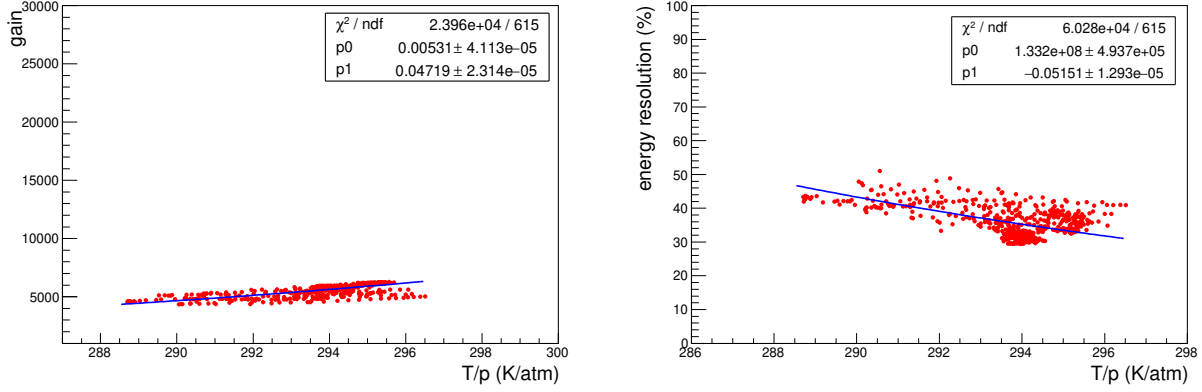


Figure 14: Correlation plots: Gain as a function of T/p (Left). Energy resolution as a function of T/p (Right). With Ar/CO₂ in the 70/30 volume ratio.

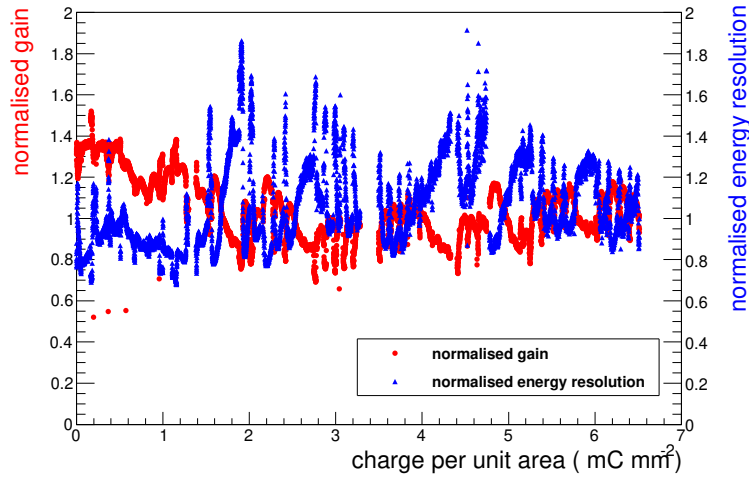


Figure 15: Variation of the normalised gain and normalised energy resolution as a function of the charge per unit area i.e. dq/dA . With Ar/CO₂ in the 70/30 volume ratio.

with X-ray of rate ~ 350 kHz from the X-ray source. The spectra are stored automatically using the ORTEC MCA at an interval of 5 minutes. Since the gain of the gas filled detector depends significantly on the ratio of the temperature and pressure (T/p), according to the relation 4 [70], the temperature (t in $^{\circ}\text{C}$) and pressure (p in mbar) are also recorded simultaneously using a data logger built in-house [67, 68]. CuteCom software package is used for automatic and continuous monitoring of the temperature and pressure [73]. After setting up all things and applying $\Delta V = 383.7$ V, the detector is kept for 5 hours for conditioning. The measurement of gain and energy resolution is continued uninterruptedly for a period of > 1200 hours after the conditioning, at a continuous X-ray radiation of 7 kHz/mm^2 . [57].

The variation of the measured gain, energy resolution and T/p are shown as a function of time in Figure 13, where $T (= t+273)$ is the absolute temperature in Kelvin and p (p in mbar/1013) is the atmospheric pressure. There is a small gap at around 600 hours as during this period the spectra are not saved but the radiation, as well as the HV to the detector were on. In a continuous operation of over 1200 hours, the gain varies between 9000 to 5000 whereas the variation of energy resolution is between 25% to 45% FWHM.

The gain vs. T/p and energy resolution vs. T/p correlation plots are drawn and fitted with functions given by equations 4 and 10 as shown in the Left and Right plots of Figure 14 respectively. Where in the following

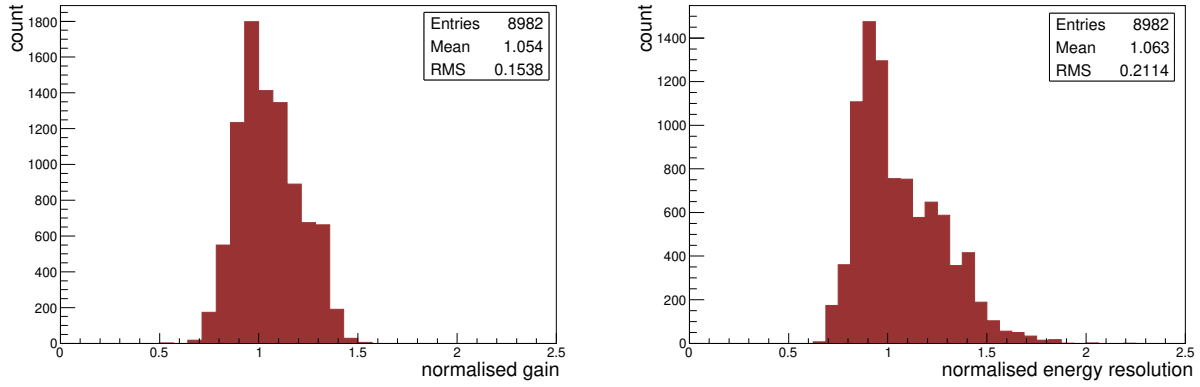


Figure 16: The distribution of the normalised gain (Left) and the normalised energy resolution (Right). With Ar/CO₂ in the 70/30 volume ratio.

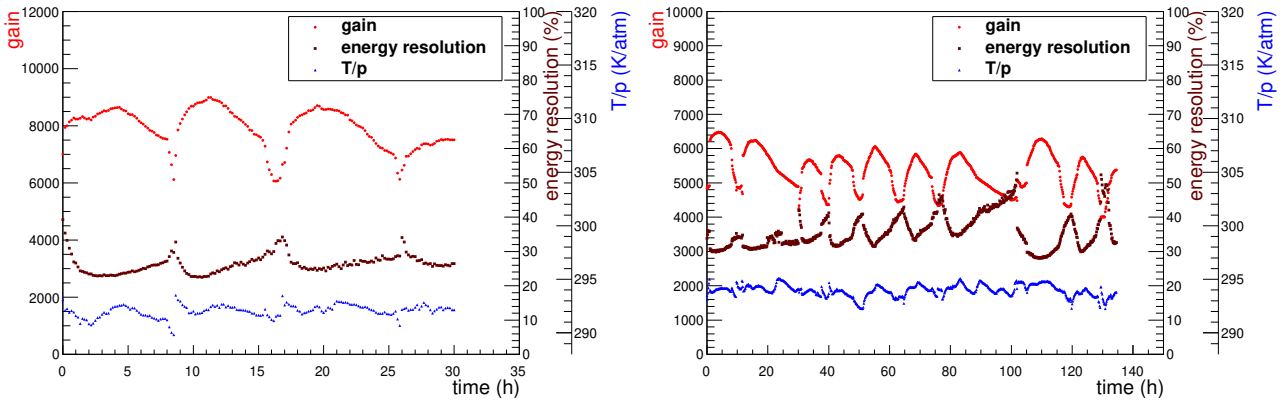


Figure 17: Gain, energy resolution and T/p as a function of time for Ar/CO₂ (80/20) gas mixture (Left) and Ar/CO₂ (90/10) gas mixture (Right).

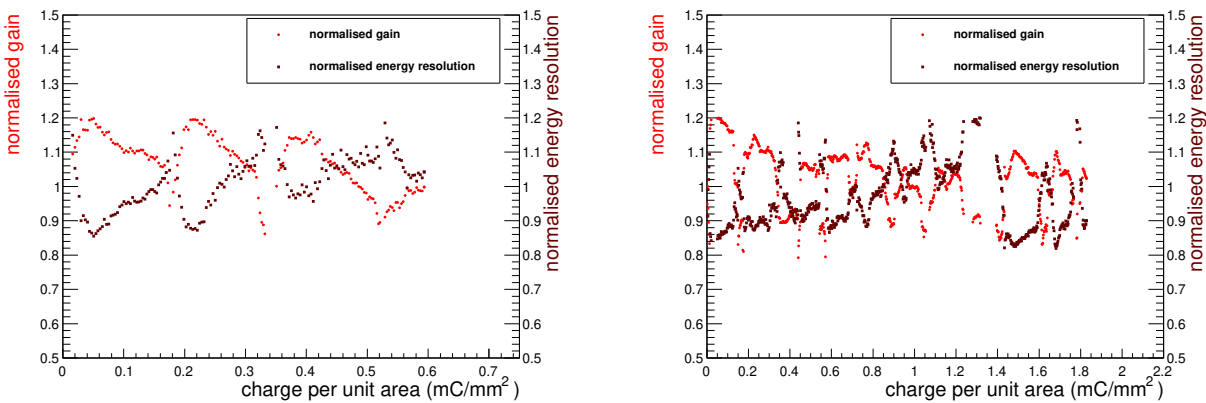


Figure 18: The normalized gain and normalized energy resolution as a function of the total charge accumulated per unit area for Ar/CO₂ (80/20) gas mixture (Left) and Ar/CO₂ (90/10) gas mixture (Right).

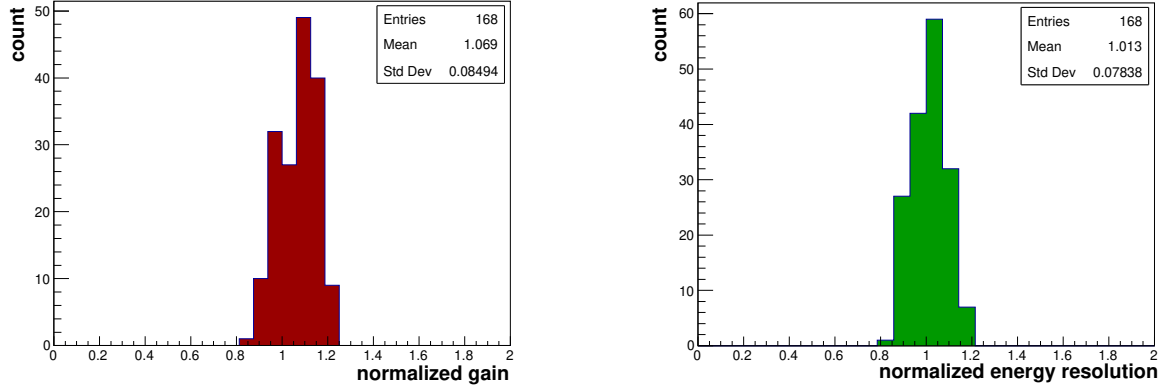


Figure 19: Distribution of the normalized gain (Left) and normalized energy resolution (Right) for Ar/CO₂ (80/20) gas mixture

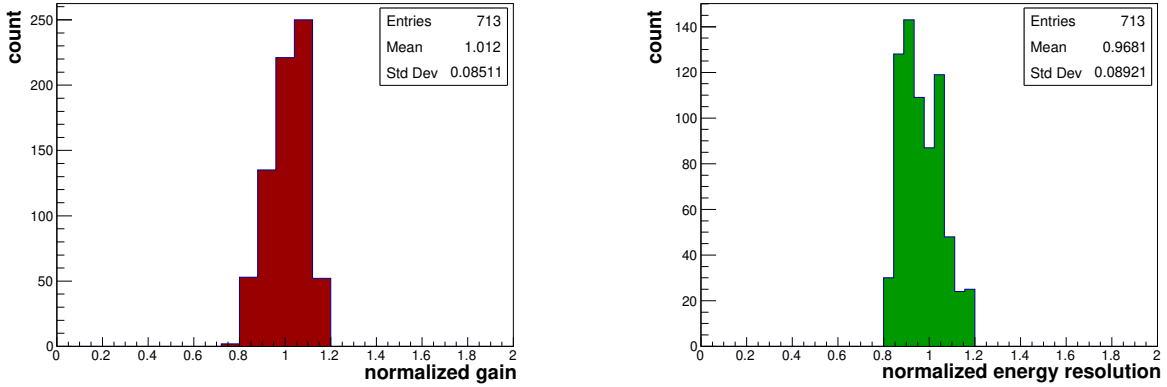


Figure 20: The normalized gain (Left) and normalized energy resolution (Right) for Ar/CO₂ (90/10) gas mixture

equation

$$\text{energy resolution} = A'e^{\left(\frac{B'}{p}\right)} \quad (10)$$

A' and B' are the fit parameters (in Figure 14 (Right) the parameters A' and B' are marked as p_0 and p_1 respectively). For gain, the parameters A and B are also marked as p_0 and p_1 respectively in Figure 14 (Left). After fitting the correlation plot, the values of the fit parameters A and B obtained, are $0.005 \pm 4.11 \times 10^{-5}$ and $0.047 \pm 2.31 \times 10^{-5}$ atm/K respectively and the values of A' and B' obtained from the fitting are $1.33 \times 10^8 \pm 4.93 \times 10^5$ and $-0.05 \pm 1.29 \times 10^{-5}$ atm/K. The measured gain and energy resolution are normalised with the gain calculated from equation 5 and 10 respectively.

To study the stability of the gain and energy resolution, the normalised gain (6) and the normalised energy resolution are plotted as a function of the total charge accumulated per unit irradiated area of the GEM detector, which is directly proportional to the time. The charge accumulated at a particular time is calculated by

$$\frac{dq}{dA} = \frac{r \times n \times e \times G \times dt}{dA} \quad (11)$$

where, r is the measured rate in Hz incident on a particular area of the detector, dt is the time in second, n is the number of primary electrons for a single X-ray photon, e is the electronic charge, G is the gain and dA is the irradiated area. For each data point, the charge is calculated in a time interval (10 minutes here) and it is summed up to get the total accumulated charge. In this test a total accumulation of charge per unit area ~ 6.5 mC/mm² is achieved. The normalised gain as a function of the total accumulated charge per unit area

is shown in Figure 15. The distribution of the normalised gain and normalised energy resolution are shown in Figure 16 Left and 16 Right respectively. The mean of the distribution for normalised gain has been found to be 1.054 with an rms of 0.15, whereas the distribution shows that after a period of > 1200 hours of continuous radiation, the mean normalised energy resolution is 1.063 with an rms of 0.21. The conclusion of this test is that, no deterioration in gain and energy resolution even after > 1200 hours of continuous operation.

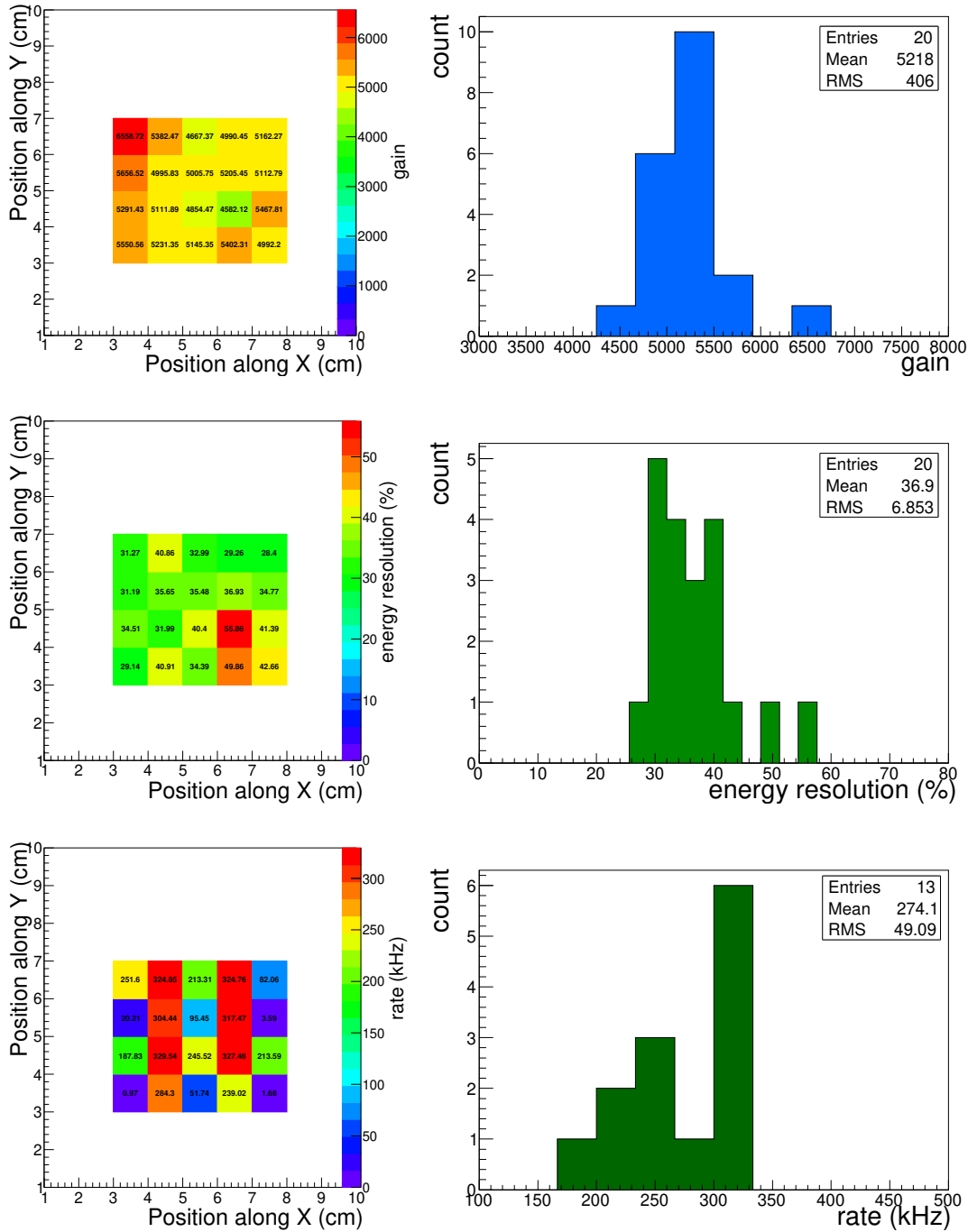


Figure 21: Gain (top), energy resolution (middle), count rate (bottom) at 20 different places on the detector and their distribution. With Ar/CO₂ in the 70/30 volume ratio.

The tests of the DM chamber with Ar/CO₂ 80/20 and 90/10 mixtures are performed at HV of - 3875 V and - 3600 V corresponding to $\Delta V \sim 359$ V and 331 V across each GEM foil respectively. The currents through the

divider chain are found to be $\sim 650 \mu\text{A}$ and $599 \mu\text{A}$. The drift, transfer and induction fields in case of Ar/CO₂ 80/20 are kept constant at 2.17 kV/cm, 3.25 kV/cm and 3.25 kV/cm respectively, whereas those fields in case of 90/10 mixture are kept at 1.99 kV/cm, 2.99 kV/cm and 2.99 kV/cm respectively. These two tests are carried out for a duration of ~ 30 hours and ~ 140 hours respectively. A perspex collimator having an area of $\sim 13 \text{ mm}^2$ is used to irradiate the chamber at a rate of $\sim 250 \text{ kHz}$ [58]. The gain and energy resolution are calculated from the Fe⁵⁵ 5.9 keV peak and then normalization is done using T/p correction as reported earlier [57].

Figure 17 Left and Right show the variation of the gain and the energy resolution of the prototype as a function of time along with the ratio of ambient temperature ($T=t+273$) and atmospheric pressure (p) for (80/20) and (90/10) gas mixtures, respectively. Figure 18 Left and Right show the variation of normalized gain and normalized energy resolution as a function of the charge accumulated per unit area for (80/20) and (90/10) gas mixtures, respectively. Figure 19 Left and Right show the distribution of the normalized gain and the normalised energy resolution for the (80/20) gas mixture and Figure 20 Left and Right show that for the (90/10) gas mixture, respectively. From Figure 19 it is observed that the mean in the normalized gain and normalised energy resolution for the (80/20) mixture is 1.069 and 1.013 with a standard deviation of 0.085 and 0.078 respectively. For (90/10) mixture the mean values in normalized gain and normalised energy resolution are 1.012 and 0.968 with a standard deviation of 0.085 and 0.089 respectively as seen from Figure 20. This test is performed to find out the difference in the coefficients for two different gas mixtures. It is found that the T/p coefficients vary with the gas composition. The numerical values of A , B (from equation 4) and A' , B' (from equation 10) as obtained from different gas mixtures are tabulated in Table 1.

Table 1: T/p coefficients A , B (from equation 4) and A' , B' (from equation 10) for different gas mixture

Gas mixture Ar/CO ₂	ΔV (Volt)	A	B atm/K	A'	B' atm/K
70/30	383.7	5.00×10^{-3} $\pm 4.11 \times 10^{-5}$	0.047 $\pm 2.31 \times 10^{-5}$	1.33×10^8 $\pm 4.93 \times 10^5$	-0.05 $\pm 1.29 \times 10^{-5}$
80/20	359	4.01×10^{-5} $\pm 0.79 \times 10^{-5}$	0.06 $\pm 0.07 \times 10^{-2}$	4.19×10^7 $\pm 5.82 \times 10^6$	-0.05 $\pm 0.05 \times 10^{-2}$
90/10	331	1.40×10^{-9} $\pm 3.91 \times 10^{-10}$	0.09 $\pm 0.1 \times 10^{-2}$	5.42×10^{11} $\pm 1.32 \times 10^{11}$	-0.08 $\pm 0.08 \times 10^{-2}$

It is to be mentioned here that during all the stability tests of GEM detectors the RH is found to be about 45-50% [74].

2.2.3 Uniformity of performance of the double mask GEM detector

For the DM module, the uniformity of gain, energy resolution and count rate is also studied with Ar/CO₂ 70/30 gas mixture. During uniformity study, a gas flow rate of 3.4 l/h is maintained and a circular collimator of diameter 8 mm is used to expose the X-ray from the Fe⁵⁵ source. Initially, the gain and energy resolution are measured from the energy spectrum and the count rate is measured from the scaler counter using the Fe⁵⁵ X-ray source, varying the potential difference ΔV across the GEM foils. ΔV is kept the same for all three GEM foils [59]. Since the experiment is performed with a radiation source that emits a constant number of particles, a plateau in the count rate is reached at the highest efficiency of the chamber. The uniformity investigation of the detector is carried out at an applied HV of - 4150 V corresponding to a $\Delta V \sim 385.9 \text{ V}$ across each GEM foil. During the uniformity investigation, the active area of the chamber is divided into 100 zones of 1 cm^2 and the gain, energy resolution and count rate are measured in a grid of 5×4 positions in the centre of the detector i.e. in 20 zones. For each position, spectra and counts are recorded for 1 minute.

Figure 21 shows the measured values of the gain, energy resolution and count rate at different places of the detector (left panel) as well as the distribution of these three parameters (right panel). For some zones where there is no readout pad corresponding to the source position, the count rate was found to be as low as 100 kHz. So for the distribution of the count rate a lower cut of 150 kHz is used. Over the measured area, the gain fluctuation is found to be $\sim 10\%$ while the fluctuation of energy resolution and count rate is $\sim 20\%$. The fluctuations in gain and energy resolution reported in Ref [63] are 8.8% and 6.7% respectively. However, they have used a collimated source of low activity. It is again to be mentioned here that a gain variation up to 25% is possible because of the intrinsic gain inhomogeneities for GEM geometry variations and also for the inhomogeneity in the gap between the individual GEM foils. This effects are extremely well described in the

References [71, 72].

3 Straw tube

Here I summarised the results from the characteristic study of a straw tube detector prototype using premixed gas of Argon and CO₂ in 70/30 and 90/10 volume ratio. In this study, the gain and the energy resolution are measured using Fe⁵⁵ X-ray source. The effect of temperature and pressure on these parameters are also studied. The same X-ray source is used to irradiate the straw and to collect the spectra. The motivation of this work is to study the rate handling capacity of straw tube detector and to measure the variation of gain and energy resolution over time or charge accumulated, using the Fe⁵⁵ X-ray spectrum. The details of the test set-up, the method of measurement and the test results are presented in this review.

3.1 Detector description and experimental set-up

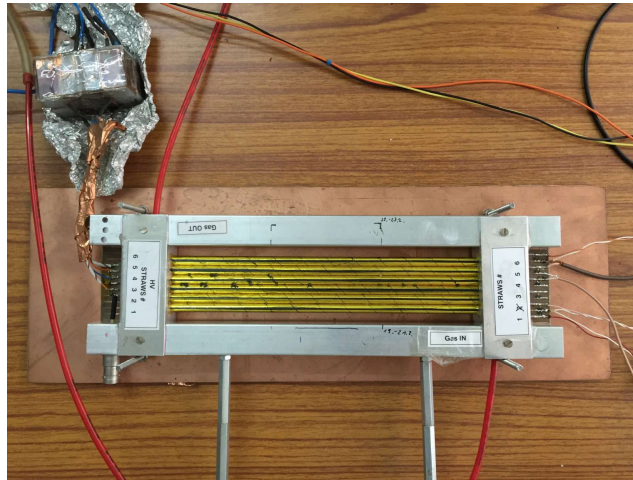


Figure 22: The straw tube prototype : 6 straws, each of diameter 6 mm and length 25 cm.

The straw tube prototype used in this study consists of 6 straws of diameter 6 mm and length 25 cm as shown in Figure 22. Pre-mixed Ar/CO₂ in 70/30 and 90/10 volume ratios are used for the different measurements. A constant gas flow rate of 3 l/h is maintained using a Vögtlin gas flow meter. The detector is tested using conventional NIM electronics. The positive HV is applied to one end of the central wire of the straws using a HV filter box and the signals are collected from the other end through a capacitor using LEMO connector. A single HV channel is used for each straw tube. The output signal from the straw is fed to a charge sensitive preamplifier (VV50-2) [64] as used in the R&D of the GEM detector. The output of the preamplifier is then fed to a linear Fan-in-Fan-out (linear FIFO) module. To measure the incident particle rate the analog signal from the linear FIFO is put to a timing SCA (Single Channel Analyser). The SCA is operated in integral mode and the lower level in the SCA is used as the threshold to the signal. The threshold is set at 1.3 V to reject all the noise. The discriminated TTL signal is fed to a TTL-NIM adapter and the output is counted using a NIM scaler. The count rate (i.e. counts per second) of the detector is then calculated. To obtain the energy spectrum, one output of the linear FIFO is fed to a Multi Channel Analyser (MCA). A schematic representation of the set-up is shown in Figure 23.

3.2 Experimental results

The count rate from the straw is measured using Fe⁵⁵ X-ray source with a gas mixture of Argon and CO₂ in 70/30 volume ratio. The source is kept on the straw tube and the count is measured for 10 minutes with and without the source for different voltage settings from 1100 V to 1750 V. The count rate is then calculated for the source only. The count rate for Fe⁵⁵ X-ray source is measured as a function of the applied HV and is plotted in Figure. 24. It is seen that a plateau is obtained from about 1600 V onwards.

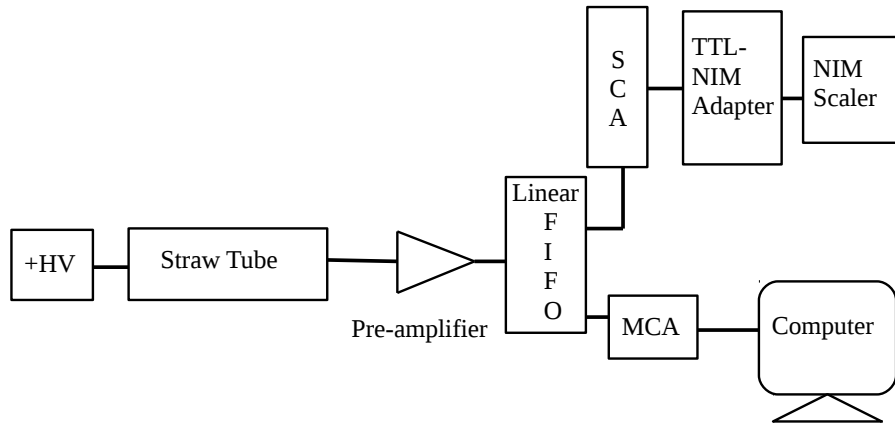


Figure 23: Schematic representation of the electronics setup for straw tube.

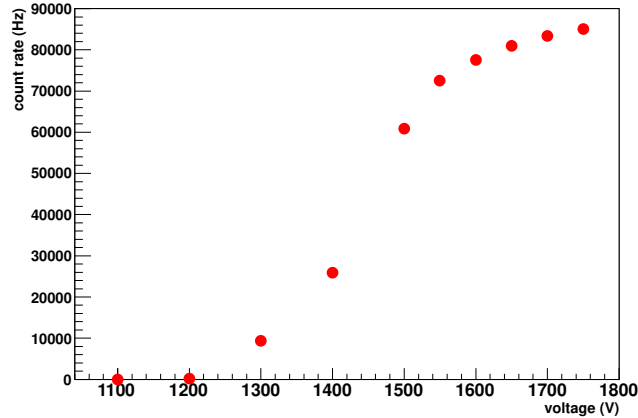


Figure 24: The count rate as a function of applied voltage for Fe^{55} source. With Ar/CO_2 in the 70/30 volume ratio.

The energy spectrum for the Fe^{55} X-rays is obtained and the gain and energy resolution are measured in the particular study. Figure 25 shows a typical energy spectrum recorded from a straw tube with Fe^{55} source at a biasing voltage of 1650 V with Ar/CO_2 in 70/30 gas mixture. In this spectrum, the main peak (5.9 keV full energy peak) and the escape peak are clearly visible and well separated from the noise peak.

The gain and energy resolution are measured by increasing the bias voltage of the straw tube detector, and obtaining the mean position of 5.9 keV peak of Fe^{55} X-ray spectrum with Gaussian fitting as done for the GEM detector using the relations 8 and 9 respectively. It is observed that the gain increases exponentially whereas the energy resolution value decreases with the increasing voltage as shown in Figure 26.

Being a gaseous detector, the gain of the straw tube depends significantly on the ratio of temperature and pressure, (T/p) . The dependence of the gain (G) of a gaseous detector on absolute temperature and pressure is given by relation 5, where the parameters A and B are to be determined from the correlation plot.

The variation of the gain as a function of temperature and pressure is also studied for the straw tube detector from the energy spectrum obtained using the same Fe^{55} source with Ar/CO_2 gas in 70/30 volume ratio. The detector is biased with 1650 V and is exposed to X-rays from the Fe^{55} source at a rate of 53 kHz and the energy spectra are recorded. Simultaneously the temperature (t in $^\circ\text{C}$), pressure (p in mbar) and relative humidity (RH in %) are also recorded using a data logger, built in-house [67]. The measurement is done for a time period of ~ 450 hours.

The gain of the detector is calculated using the formula given in equation 8. The variation of the measured

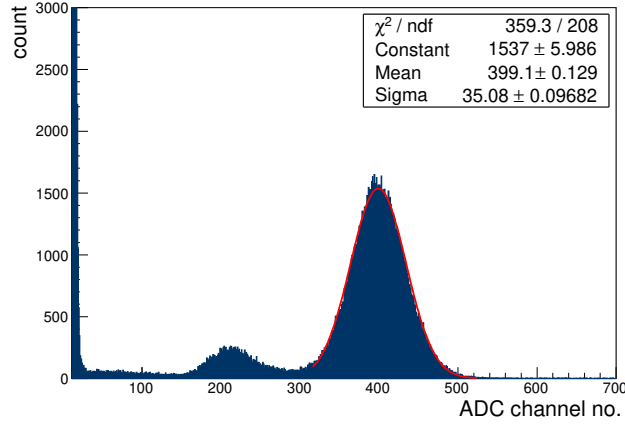


Figure 25: Energy spectrum of the straw tube detector. The red line is the Gaussian fitting curve to the 5.9 keV peak. With Ar/CO₂ in the 70/30 volume ratio.

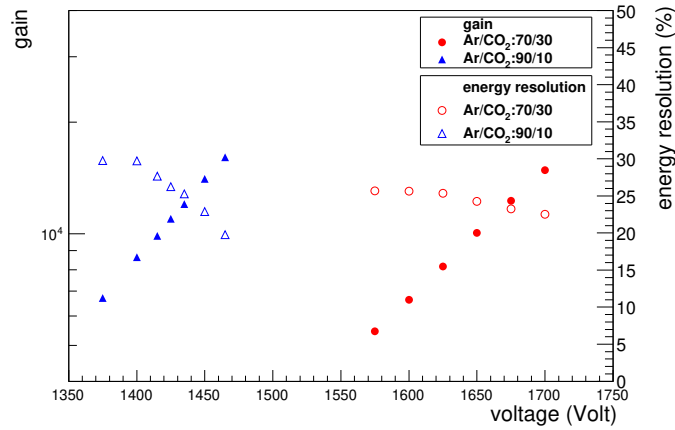


Figure 26: The Gain and the energy resolution as a function of the voltage for both Ar/CO₂ 70/30 and 90/10 mixtures. The error bars are smaller than the symbols.

gain is plotted as a function of the period of operation in Figure 27. The variation of the T/p as a function of the total period of operation is also plotted in Figure 27, where T (= t+273) is the absolute temperature in Kelvin and p (p in mbar/1013) is in the unit of atmospheric pressure.

The correlation plot, i.e. the gain is plotted as a function of T/p and fitted with the function given by equation 4 and is shown in Figure 28 (in Figure 28 the parameters A and B are marked as p0 and p1 respectively).

The values of the fit parameters A and B obtained, are 187.8 ± 11.18 and 0.015 ± 0.0002 atm pr/K respectively. Using the fit parameters, the gain is normalised by using relation 6.

To check the stability of the detector, the normalised gain is plotted as a function of the total charge accumulated per unit irradiated length of the detector which is directly proportional to the time. The charge accumulated at a particular time is calculated by

$$\frac{dq}{dL} = \frac{r \times n \times e \times G \times dt}{dL} \quad (12)$$

where r is the measured rate in Hz incident on a particular length of the detector, dt is the time in second, n is the number of primary electrons for a single X-ray photon, e is the electronic charge, G is the gain and dL is the irradiated length of the straw. The normalised gain as a function of the charge accumulated per unit length is shown in Figure 29. There is a fluctuation around 1 in the normalised gain value as shown in Figure 29. The

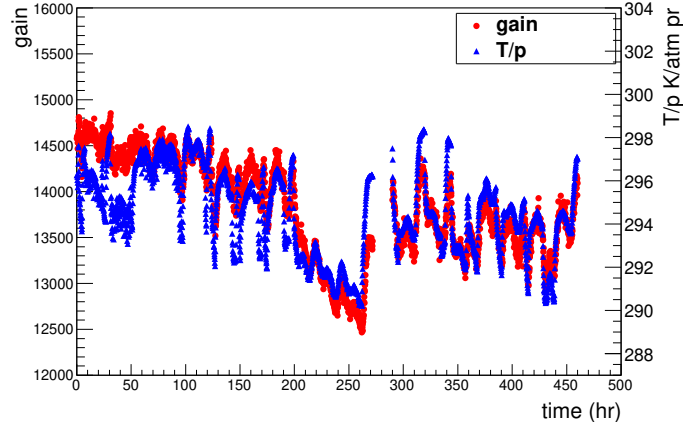


Figure 27: Variation of the measured gain and T/p as a function of the time. The error bars are smaller than the symbols for gain. With Ar/CO₂ in the 70/30 volume ratio.

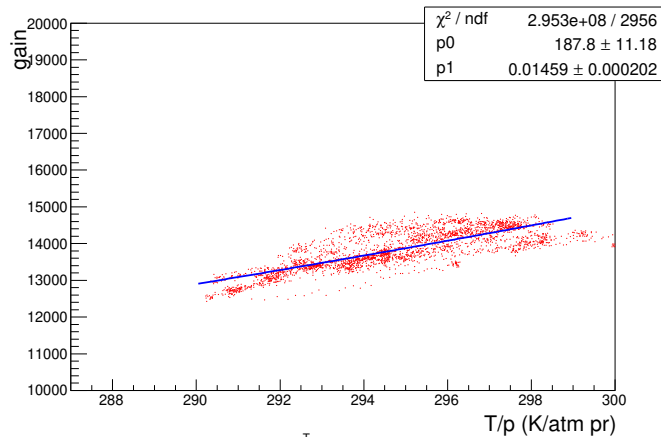


Figure 28: Correlation plot: Variation of the gain as a function of T/p. With Ar/CO₂ in the 70/30 volume ratio.

distribution of the normalised gain is shown in Figure 30. The mean normalised gain is found to be 0.998 with a standard deviation of 0.021 for a continuous operation of 450 hours, as shown in Figure 30. In this study, an accumulation of charge per unit length ~ 32 mC/mm is achieved. No deterioration in the gain of the detector is observed. It may be mentioned here as an example that, at a chosen gain of 10^4 , for minimum ionising particles (MIP) the charge accumulated along the length in the straws at the 3rd station of CBM-MUCH for three months of operation is estimated to be 0.86 mC/mm.

In this study also, the energy resolution is measured for each spectrum. The energy resolution as a function of time is shown in Figure 31 (Left). The distribution of energy resolution as shown in Figure 31 (Right) shows that during this time of ~ 450 hours the mean energy resolution is 20.27% with a standard deviation of 0.21%.

The variation of the gain and the energy resolution of the straw tube detector is measured by varying the rate of incident X-ray photons on the detector. A collimator made with perspex is used to change the rate of emitted X-ray falling on the chamber from the Fe⁵⁵ source. The collimator arrangement is such that the active part of the source can be made misaligned with the opening of the collimator to vary the rate of particles incident on the detector. In this way the total number of particle reaching the detector changes but the exposed area remains the same.

The energy spectrum is obtained for each collimator settings. These measurements are performed with both Ar/CO₂ 70/30 and 90/10 gas mixtures. For Ar/CO₂ 70/30 the measurements are performed keeping the HV to

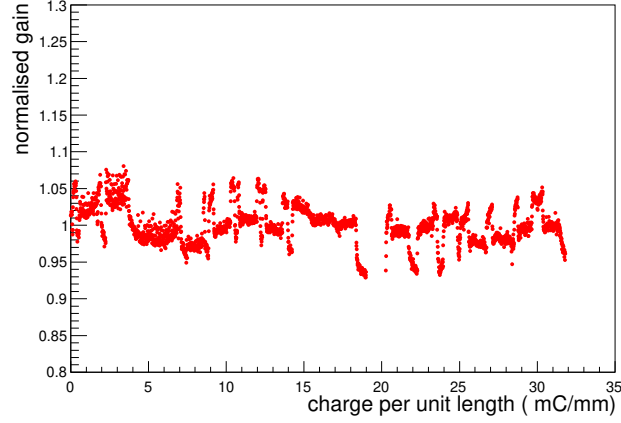


Figure 29: Variation of the normalised gain as a function of the charge per unit length i.e. dQ/dL . The error bars are smaller than the symbols. With Ar/CO₂ in the 70/30 volume ratio.

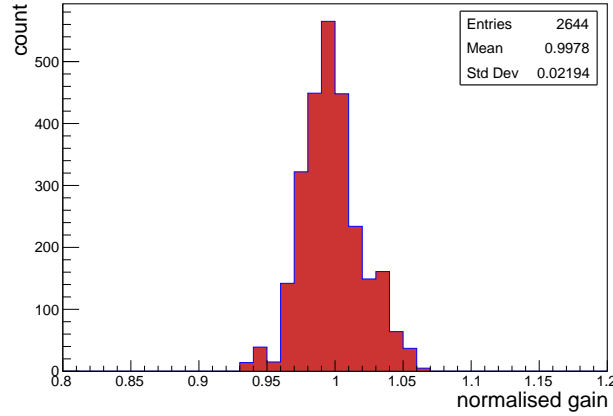


Figure 30: The distribution of the normalised gain. With Ar/CO₂ in the 70/30 volume ratio.

the straws at 1650 V and 1700 V whereas for Ar/CO₂ 90/10 it is done for HV 1400 V and 1450 V. For Ar/CO₂ 70/30 the gain and energy resolution are measured from a rate of about 200 Hz/mm to about 3×10^4 Hz/mm and that for Ar/CO₂ 90/10 are performed for about 100 Hz/mm to about 6×10^4 Hz/mm. Measured gain and energy resolution as a function of X-ray rate per unit length are shown in Figure 32 and Figure 33 respectively. It is observed that for Ar/CO₂ 70/30 the gain and the energy resolution remain constant up to a rate of about 2×10^4 Hz/mm then the gain decreases and the energy resolution value increases with the rate because of the space charge effect. A similar effect is observed for Ar/CO₂ 90/10 as well, where the gain and energy resolution remain constant up to a rate of about 3.2×10^4 Hz/mm.

For higher rates, the gain (G) is fitted with a function [69]

$$G = P e^{-Q \cdot R} \quad (13)$$

where P and Q are the fit parameters and R is the rate.

For higher rates, the energy resolution is also fitted with a function

$$\text{energy resolution} = P' e^{Q' \cdot R} \quad (14)$$

where P' and Q' are the fit parameters and R is the rate.

The numerical values of P , Q , P' and Q' as obtained from different set of measurements are tabulated in Table 2.

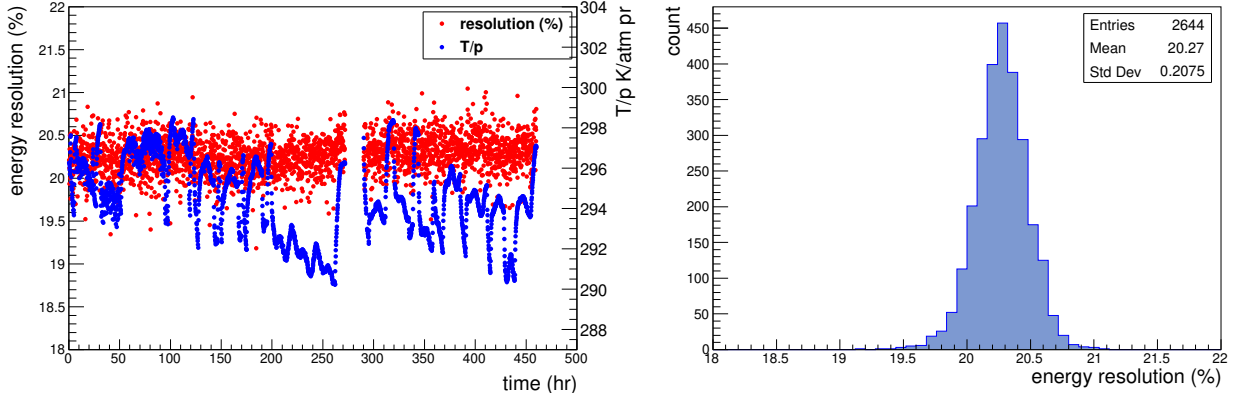


Figure 31: (Left) Variation of the energy resolution as a function of time. The error bars are smaller than the symbols. (Right) The distribution of the % energy resolution. With Ar/CO₂ in the 70/30 volume ratio.

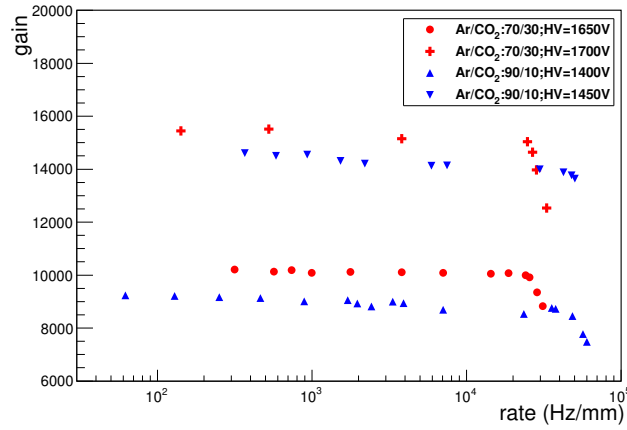


Figure 32: Gain as a function of rate for both Ar/CO₂ 70/30 and 90/10 mixtures. The error bars are smaller than the symbols.

It is observed that for Ar/CO₂ 70/30 gas mixture the detector is operated at a relatively higher voltages and in this case decrease of gain with rate started at a relatively lower rate. However, it is to be mentioned here that the observation of such space charge effects is well known and very common in case of wire chambers, that is why these detectors cannot be operated at very high gains or very high rates. Therefore, new types of gaseous detectors like the GEM is developed to overcome this drawback.

Table 2: Values of the fit parameters.

Gas mixture Ar/CO ₂	Voltage (Volt)	P	Q	P'	Q'
70/30	1650	1.58×10^4	1.86×10^{-5}	4.72	7.07×10^{-5}
70/30	1700	2.75×10^4	2.38×10^{-5}	4.25	6.98×10^{-5}
90/10	1400	1.08×10^4	5.67×10^{-6}	24.77	6.70×10^{-6}
90/10	1450	1.53×10^4	2.26×10^{-6}	21.41	2.71×10^{-6}

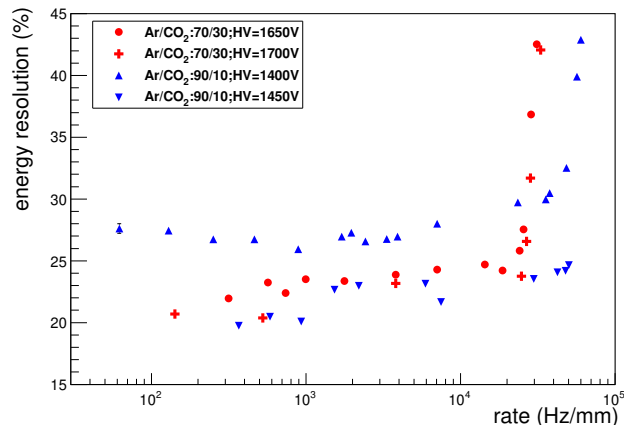


Figure 33: Energy resolution as a function of rate for both Ar/CO₂ 70/30 and 90/10 mixtures. The error bars are smaller than the symbols.

4 Resistive Plate Chamber

Since the invention of the Resistive Plate Chambers (RPCs) [26] as a cost effective technology that can be used to build large area granular, reasonably fast and moderate to high rate capable detectors, it has found use not only in a large number of high energy physics experiments such as BABAR, ALICE, ATLAS, CMS, STAR, HADES [34, 36, 37, 76, 77, 78, 80] as trigger, Time of Flight (TOF) and tracking devices but also in several cosmic ray experiments [81, 82] and Neutrino experiments such as OPERA, DAYABAY [83, 84, 49]. Future experiments such as Compressed Baryonic Matter (CBM) at FAIR also propose to use RPCs as one of the key detectors [85].

Keeping in mind the possibility of using RPCs as future high rate capable (~ 15 kHz/cm²) tracking detectors [86], we have taken up an initiative to study the characteristics of RPC prototypes built using carbon-loaded Polytetrafluoroethylene (PTFE) material commonly known as Teflon and also with locally available bakelite plates with moderate bulk resistivity. The prototypes are tested with 100% Tetrafluoroethane ($C_2H_2F_4$) gas for the first time in this work.

4.1 RPC with PTFE

4.1.1 Detector description and experimental set-up

Initially, a prototype RPC is fabricated with a carbon-loaded Polytetrafluoroethylene (PTFE) material commonly known as Teflon. This particular sample is 25% carbon-filled, having a bulk resistivity of $10^5 \Omega \cdot \text{cm}$ (at 23°C temperature and 60% Relative humidity). The bulk resistivity is calculated by measuring the leakage current through a sample after the application of voltage. The method of bulk resistivity measurement is the same as described in Ref [75]. It is to be mentioned here that carbon-loaded PTFE or any other carbon-loaded resistive plate can be tuned according to the requirement of resistivity by changing the carbon-content and these resistive plates can be used for high rate RPC fabrication. The relationship between carbon-content and the resistivity is non-linear and substantial R&D needs to be done on this front alone to find suitable materials.

Two 15 cm \times 15 cm plates of thickness 1 mm are used to build this detector. 2 mm gas gap is maintained using four edge spacers of dimension 1 cm \times 15 cm and four button spacers of 1 cm diameter. Two gas nozzles are used for the gas inlet and outlet. The flat part of the gas nozzle is also of thickness 2 mm and a hole of 1 mm diameter is drilled in it for gas flow. All the spacers and gas nozzles are made with polycarbonate. The measured surface resistivity of the carbon-loaded PTFE is found to be 20 k Ω /□. Since the surface resistivity of carbon-loaded PTFE is very low, the material is not coated with graphite for the distribution of high voltage. As the surface of the material is found to be smooth by visual inspection, we have not used any oil coating in this case.

100% Tetrafluoroethane ($C_2H_2F_4$) is used as the chamber's sensitive gas. The induced signal is collected by orthogonal pick-up strips placed on two sides of the chamber. There are four copper strips of dimension

2.5 cm \times 15 cm with a separation of 2 mm, at the central part of the module on each side. The copper pick-up strips are pasted on a G-10 board of thickness 3 mm and dimension 15 cm \times 15 cm. The ground plane of the pick-up panel is made of aluminium foil. The complete RPC module along with the pick up strips are shown in Figure 34 (Left).

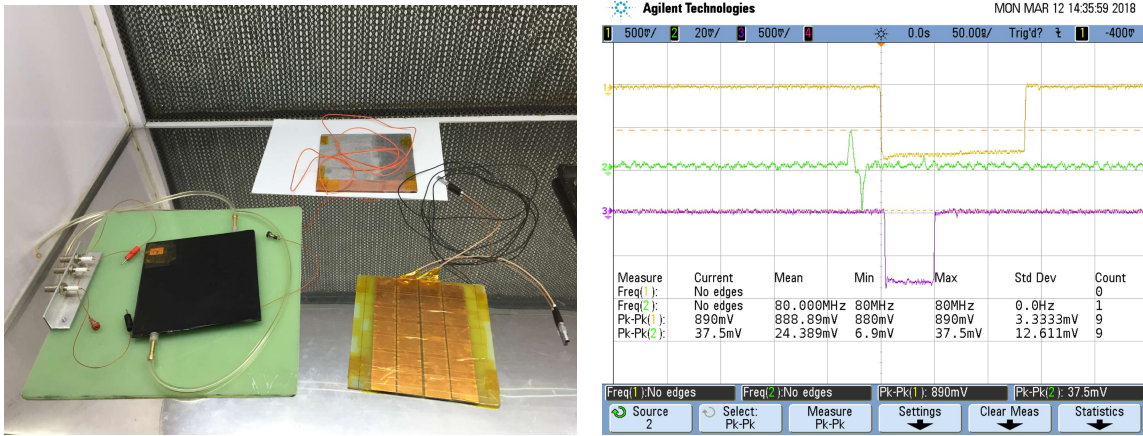


Figure 34: (Left) Complete RPC along with copper pick-up strips. (Right) Signal after the preamplifier.

A differential voltage is applied to the diagonally opposite corners of two sides of the chamber to produce the electric field inside the gas gap. A charge sensitive preamplifier (VV50-2) [64] which is used for the GEM detector and straw tube, is also used here for the signal collection. In Figure 34 (Right), the green line represents the signal after the preamplifier, which is taken from the positive plane of the detector. There was always a reflected negative part in each signal because of impedance mismatch and this negative part is used for further processing of the signal using a leading edge discriminator (LED). For efficiency measurement, a cosmic ray test set-up is used placing two plastic scintillator detectors of dimension 20 cm \times 20 cm and 2 cm \times 10 cm above the chamber and one with dimension 10 cm \times 10 cm below it. Effectively an overlapping window of area 2 cm \times 10 cm is available for triggering purpose. The coincidence signals from these three scintillator detectors are taken as the master trigger and shown in Figure 34 Right (yellow). The width of the trigger is set to 120 ns. The discriminated RPC signal shown in magenta in Figure 34 (Right) is taken in coincidence with the master trigger to get a four-fold signal. The three-fold master trigger and the four-fold signals are counted using a NIM scaler. Only the discriminated RPC signals are also counted to measure the noise rate.

4.1.2 Results

In this study, the prototype chamber is tested for V-I characteristics, the variation of the noise rate and efficiency as a function of the applied voltage. Equal voltages of opposite polarities are applied on two planes of the module and the leakage current is measured for each settings. The V-I characteristic of the module is shown in Figure 35 (Left). Although the current increases with increasing voltage but no sharp breakdown is observed for this chamber.

The three-fold trigger signals, four-fold signals and the discriminated singles counts from the RPC are counted for 30 minutes for each voltage setting. The singles count rate is divided by the area of a strip and the count rate per unit area is calculated which is shown as a function of voltage in Figure 35 (Right). It is seen that the noise rate increases with voltage. The ratio of the four-fold count rate to the three-fold count rate is the efficiency and that as a function of the voltage is also shown in Figure 35 (Right). The efficiency also increases with increasing applied voltage. At a voltage of 4 kV, typical values of efficiency and noise rate are found to be \sim 60% and 0.02 Hz/cm² respectively. This value of efficiency is quite low considering an efficiency of 90 % of a typical single gap RPC. However, for this detector, discharges happen beyond the high voltage of 4 kV. Because of this drawback, another prototype is built using locally available bakelite plates to continue with the R&D of the RPCs. The bakelite plates of the new RPC detector has moderate bulk resistivity.

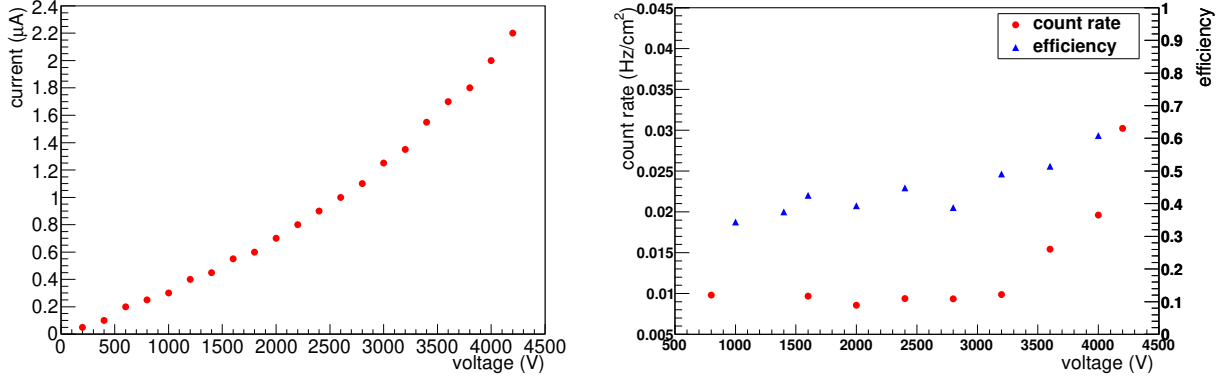


Figure 35: (Left) V-I characteristics. (Right) Noise rate and Efficiency Vs. voltage. Gas: 100% $\text{C}_2\text{H}_2\text{F}_4$.

4.2 RPC with bakelite

4.2.1 Detector description and experimental set-up

This prototype is built with two 2 mm thick bakelite plates, each having dimension $30\text{ cm} \times 30\text{ cm}$ and bulk resistivity $3 \times 10^{10}\ \Omega\text{ cm}$ (at 22°C temperature and 60% Relative humidity) and without any linseed oil coating inside. The gas gap is maintained with four edge spacers having width 1 cm and thickness 2 mm and one button spacer having 1 cm diameter, thickness 2 mm. Both kinds of spacers are made of polycarbonate (resistivity $\sim 10^{15}\ \Omega\text{ cm}$). The surface resistivity of the graphite layer is measured to be $\sim 500\text{ k}\Omega/\square$. Two $1\text{ cm} \times 1\text{ cm}$ copper tapes are used at two diagonally opposite corners to apply the HV. HV of opposite polarities is applied on two sides. To collect the signals, copper pick-up panels are used. They are made of 2.5 cm wide strips with a separation of 2 mm between two consecutive ones.

This prototype is also tested with 100% Tetrafluoroethane ($\text{C}_2\text{H}_2\text{F}_4$) but the current is also measured with a mixture of Ar/CO_2 (70/30). The signals from the pick-up strips are fed to a 10X fast amplifier and subsequently to the leading edge discriminator (LED). The cosmic ray master trigger is made using three fast plastic scintillators (as described in Sec. 4.1.1). Among them, two scintillators (with dimensions $10\text{ cm} \times 10\text{ cm}$ (SC 1) and $2\text{ cm} \times 10\text{ cm}$ (SC 2) respectively) are placed above and one (with dimension $20\text{ cm} \times 20\text{ cm}$ (SC 3)) is placed below the RPC module. The scintillators make the trigger window of area $2\text{ cm} \times 10\text{ cm}$. Thresholds to the discriminators are set to -15 mV for all the scintillators as well as for the RPC. The width of the 3-Fold scintillator master trigger is set to 150 ns. Finally, the discriminated RPC signal from one single strip is taken in coincidence with the 3-Fold master trigger and a 4-Fold NIM signal is obtained. The ratio of the 4-Fold signal and the 3-Fold scintillator signal is defined as the efficiency of the detector. The single RPC signals are also counted for a particular duration and the rate is defined as the noise rate of the chamber.

To measure the timing properties of the RPC, the same set-up is used. The discriminated RPC signal is stretched by a dual timer and fed as the START signal of the Time to Amplitude Converter (TAC). The 3-Fold scintillator coincidence signal is taken as the STOP signal input of the TAC. The output of the TAC is fed to the Multi Channel Analyser (MCA) and the spectra are stored in a Personal Computer (PC). Figure 36 shows the schematic of the set-up for testing the RPC module using cosmic rays.

During the whole measurement, the temperature and relative humidity inside the laboratory are maintained at $\sim 18\text{-}20^\circ\text{C}$ and 37-40% respectively, whereas the atmospheric pressure is monitored to be 1009-1020 mbar.

4.2.2 Results

In this work, the efficiency, noise rate, time difference of RPC signal and the master trigger and time resolution of an oil-less bakelite RPC as a function of voltage are measured with cosmic rays. The detector current as a function of the applied voltage is shown in Figure 37. It is visible that initially the current increases slowly with the voltage and above 8 kV the increase becomes rapid. At 8 kV voltage difference across the gap, the signal of amplitude $\sim 10\text{-}15\text{ mV}$ is observed in the DSO at $50\ \Omega$ termination. The result of the current is compared with the one obtained using Ar/CO_2 gas in 70/30 volume ratio. Sharp breakdown in the V-I characteristics resulted with Ar/CO_2 at a lower voltage (4.5 kV) compared to that with the Tetrafluoroethane.

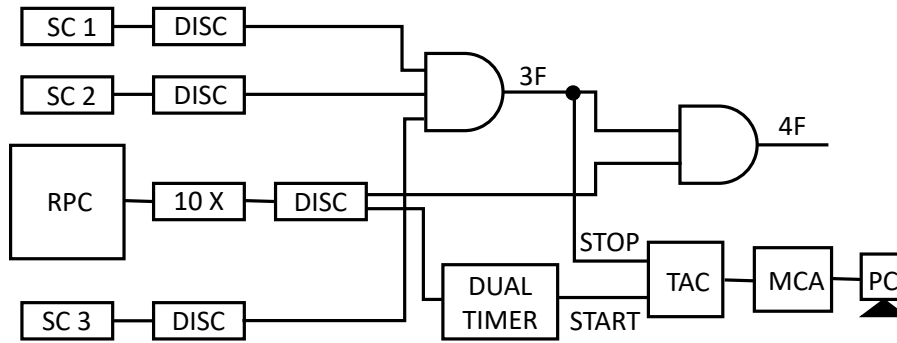


Figure 36: Schematic representation of the cosmic ray test setup for efficiency and time resolution measurement. SC 1, SC 2 and SC 3 are the plastic scintillation detectors of dimensions 10 cm × 10 cm, 2 cm × 10 cm and 20 cm × 20 cm respectively. DISC, 10 X, TAC, MCA and PC are the discriminators, 10X fast amplifier, Time to Amplitude Converter, Multi Channel Analyser and Personal Computer respectively.

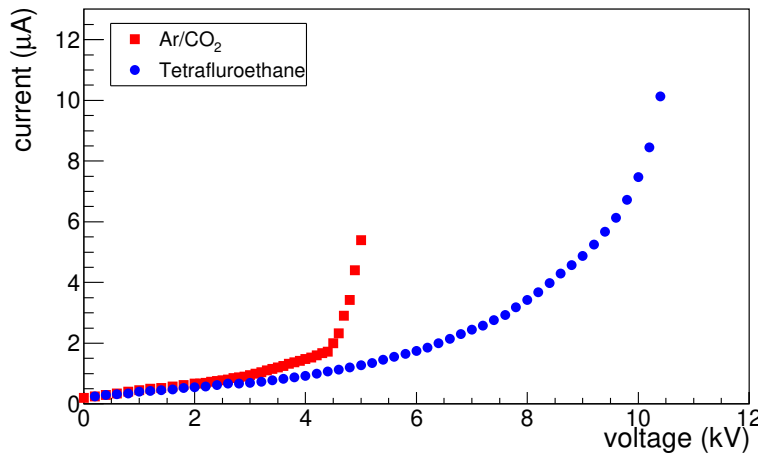


Figure 37: The V-I Characteristics of RPC with two gas mixtures.

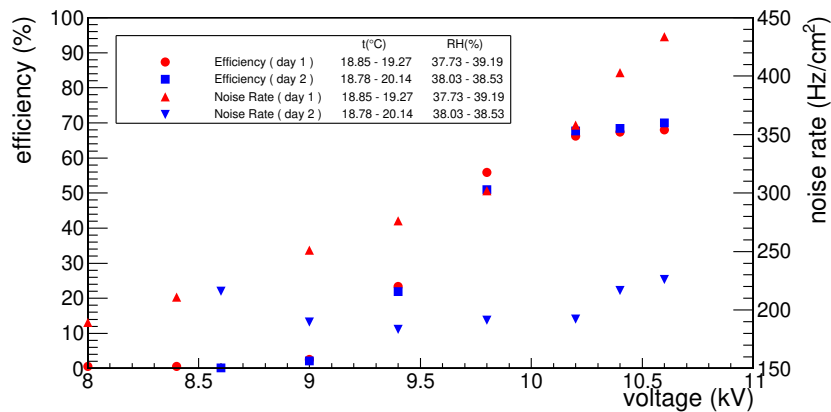


Figure 38: Efficiency and noise rate as a function of voltage with 100% C₂H₂F₄.

The noise rate as a function of voltage is measured for two consecutive days with 100% C₂H₂F₄, keeping the discriminator threshold at -15 mV and the results are shown in Figure 38. It is seen that for both days, the noise rate increases with applied voltage but on the second day, the noise rate is found to be much less than that of the first day, because of better conditioning. The conditioning is done with continuous gas flow and keeping 4 kV across the gas gap over-night. It is to be mentioned here that, for linseed oil treated bakelite

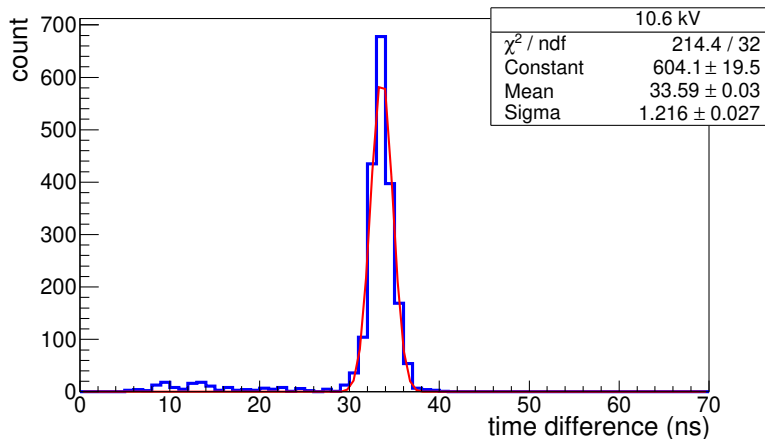


Figure 39: Time spectrum of RPC at a differential voltage of 10.6 kV across the gas gap. Gas: 100% $\text{C}_2\text{H}_2\text{F}_4$.

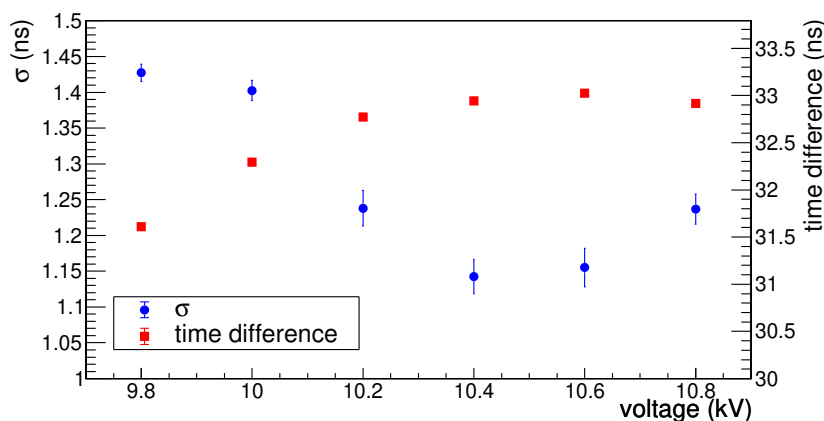


Figure 40: Time resolution and time difference of RPC signal and master trigger as a function of voltage. Gas: 100% $\text{C}_2\text{H}_2\text{F}_4$.

RPCs the noise rate is found to be two orders of magnitude better in some cases [87] under cosmic ray test and even three orders of magnitude for streamer operated RPCs with higher resistivity [88, 89, 90].

The efficiency as a function of voltage is also shown in Figure 38 for two consecutive days with 100% $\text{C}_2\text{H}_2\text{F}_4$. From Figure 38 it can also be seen that the efficiency starts increasing from 9 kV and saturates at a value of $\sim 70\%$ from 10.2 kV onwards. The same result is observed on both days.

While measuring the time resolution the RPC signal is stretched to 500 ns to avoid the effect of double or reflection pulses if there is any. The full scale of the TAC is set to 100 ns. The typical time spectrum for the RPC at 10.6 kV is shown in Figure 39. The distribution of the time difference between the RPC signal and the master trigger is fitted with the Gaussian function. Using the σ of the distribution and subtracting the contribution from the scintillator in quadrature the intrinsic time resolution of the RPC is calculated.

The time difference of the RPC signal with respect to the master trigger and the time resolution (σ) of the RPC as a function of the applied voltage are shown in Figure 40. Since the RPC signal is used as the START signal and with the increase of the applied voltage the electric field inside the RPC becomes stronger, electrons travel faster and the signals arrive earlier. As a result, with the increase of applied voltage, the time difference increases and reaches a plateau from 10.2 kV onwards. The time resolution (σ) decreases with the increase of applied voltage and a value of ~ 1.2 ns is obtained from 10.2 kV.

5 Summary and outlook

In this review I have summarised the R&D done in the detector laboratory of Bose Institute, Kolkata, on the gaseous detectors for the high energy physics experiments. This program includes R&D of GEM detector, Straw

tube and RPC.

A single mask triple GEM detector prototype is built and tested with a gas mixture of Ar/CO₂ of 70/30 volume ratio. The long-term stability test of this detector is performed using Fe⁵⁵ X-ray source. The gain is measured and normalised for the T/p effect. In the analysis, the rate of the X-ray from the source is modified according to the radioactive decay law. However, in the 750 hours of the long-term study, the rate decreased from 350 kHz to 342.4 kHz which is only 2.17% of the starting value. In this measurement, only a fluctuation about the mean value of 1.003 in the normalized gain is observed after T/p correction. No ageing is observed till an accumulation of charge per unit area > 12.0 mC/mm² [56]. From these results, it can be concluded that, triple GEM detectors can safely be used in high energy physics experiments where the long-term stability of the detector is an essential criterion.

Systematic studies on the stability of the gain and the energy resolution of a double mask triple GEM detector in long-term operation under a high rate of X-ray irradiation is also performed with Ar/CO₂ gas mixture in 70/30 volume ratio and using the conventional NIM electronics. In this study, the same Fe⁵⁵ source is used to irradiate the chamber as well as to measure the gain and energy resolution at an interval of 10 minutes. Using a collimator, the rate of the incident X-ray is fixed to ~ 350 kHz on an area of ~ 50 mm² of the GEM detector equivalent to a rate of 0.7 MHz/cm². In this study, for the first time the detector is continuously exposed to a high rate of X-ray radiation for > 1200 hours. To collect the signals from the detector a charge sensitive preamplifier (VV50-2) is used with a gain of 2 mV/fC and a shaping time of 300 ns. In a continuous operation of > 1200 hours or an equivalent accumulated charge per unit area of ~ 6.5 mC/mm² the mean normalised gain and the mean normalised energy resolution are found to be 1.054 with an rms of 0.15 and 1.063 with an rms of 0.21 respectively [57] and the prototype did not show any significant degradation in performances. Stability test of gain and energy resolution of the double mask GEM prototype is also carried out with Ar/CO₂ 80/20 and 90/10 gas mixtures. Using a collimator, the detector is irradiated with a particle flux of ~20 kHz/mm² for ~30 hours with Ar/CO₂ 80/20 gas mixture and for ~140 hours with Ar/CO₂ 90/10 gas mixture which are equivalent to a charge accumulation of ~ 0.6 mC/mm² and ~ 1.8 mC/mm², respectively [58]. No degradation is observed in gain and energy resolution other than a fluctuation of ~10% after the long-term exposure to X-ray.

The characteristics of the GEM detector will not be the same over its active area. It is to be mentioned here that a gain variation up to a few percent is possible due to the intrinsic inhomogeneity in the geometry of the GEM holes and the gaps between the GEM foils. In this study, the gain, energy resolution and count rate are measured at 20 places on the active area of the triple GEM detector prototype by moving a Fe⁵⁵ X-ray source manually to check the uniformity. For each measurement, an area of ~ 50 mm² was exposed by the 5.9 keV X-ray. Over the measured area, the gain fluctuation is found to be ~ 10% while the fluctuation of energy resolution and count rate is ~ 20% [59].

A systematic study on the characterisation of the straw tube detector is performed using conventional NIM electronics. In this study, different Ar/CO₂ gas mixtures are used. The gain and energy resolution are measured from the energy spectrum obtained using Fe⁵⁵ X-ray source. To check the effect of temperature and pressure on the gain and energy resolution, a continuous measurement is performed. The same Fe⁵⁵ X-ray source is used to irradiate the detector as well as to obtain the spectrum. The measured gain is normalised by T/p corrected gain. The normalised gain is found to be stable with an average value of 0.998 with a standard deviation of 0.021 for a duration of ~ 450 hours which is equivalent to an accumulation of charge per unit length ~ 32 mC/mm. In this study, the variation of gain and energy resolution of the straw tube detector with X-ray rate are also measured for the first time in a laboratory. The gain and the energy resolution remain constant up to a rate of about 2×10^4 Hz/mm and 3.2×10^4 Hz/mm for Ar/CO₂ 70/30 and 90/10 respectively [60]. Beyond these quoted values gain decreases and the energy resolution increases with the increase of rate because of the space charge effect.

For the RPC R&D at the laboratory of Bose Institute, a single gap RPC prototype is fabricated with a very low resistive carbon-loaded PTFE plate commonly known as Teflon, to improve the rate handling capability. The detector is tested in the avalanche mode using 100% Tetrafluoroethane (C₂H₂F₄) as the sensitive gas. A charge sensitive preamplifier is used for signal collection. The V-I characteristics, variation of noise rate and efficiency as a function of voltage are studied. At a voltage of 4 kV, an efficiency of ~ 60% is achieved [61].

An oil-less single gap RPC prototype is also built with indigenous bakelite plates having a bulk resistivity $3 \times 10^{10} \Omega \text{ cm}$. The chamber is tested in the avalanche mode with 100% Tetrafluoroethane gas. With this prototype, an efficiency ~ 70% and time resolution 1.2 ns (σ) are obtained from an applied voltage of 10.2 kV onwards [62]. Investigation of the reason behind lower efficiency is going on. One probable reason for the limitation in the efficiency is the voltage drop on the electrodes because of the high current. Other

Tetrafluoroethane based conventional gas mixtures will be tried in near future. Estimation of the induced signal charge and the long-term stability test of this particular chamber is also in the future plan.

High rate handling capability is one of the crucial factors for detectors to be used in many current and future high energy physics experiments. In that direction, we are searching for indigenous bakelite plates with better surface smoothness and lower resistivity.

Acknowledgements

Firstly, I would like to thank my students Mr. Sayak Chatterjee, Mr. Arindam Sen and Ms. Shreya Roy for doing the work meticulously, taking data, analysing data and making plots.

We would like to thank the RD51 collaboration for the support in building and initial testing of the chamber in the RD51 laboratory at CERN. We would like to thank Dr. A. Sharma, Dr. L. Ropelewski, Dr. E. Oliveri and Dr. Chilo Garabatos of CERN and Dr. C.J. Schmidt and Mr. Jörg Hehner of GSI Detector Laboratory and Mr. Dipanjan Nag, Mr. Rathijit Biswas, Prof. Sanjay K. Ghosh, Prof. Sibaji Raha, Prof. Supriya Das, Prof. Rajarshi Ray, Dr. Sidharth K. Prasad, Dr. R. P. Adak of Bose Institute for valuable discussions and suggestions in the course of all the studies.

Additionally we would also like to thank Late Prof. Vladimir Peshekhonov of JINR, Dubna, Dr. Subhasis Chattopadhyay, Mr. J. Saini of VECC, Kolkata, Dr. Christian J. Schmidt of GSI Detector Laboratory for valuable discussions in the course of the study on straw tube.

I would like to thank Mr. Sayan Chakraborty, Mr. Shibnath Shaw and Ms. Nilanjana Nandi for some valuable measurements. I would also like to thank Dr. Arindam Roy of Department of Particle Physics and Astrophysics, Weizmann Institute of Science for providing the PTFE plates for RPC.

This work is partially supported by the research grant SR/MF/PS-01/2014- BI from DST, Govt. of India, and the research grant of CBM-MUCH project from BI-IFCC, DST, Govt. of India. S. Biswas acknowledges the support of DST-SERB Ramanujan Fellowship (D.O. No. SR/S2/RJN-02/2012) and Intramural Research Grant provided by Bose Institute. I also acknowledge the support of DST-SERB Ramanujan Fellowship (D.O. No. SR/S2/RJN-02/2012). I would like to thank Mrs. S. Rudra for valuable discussions on the work and to write this article.

References

- [1] F. Sauli, Nucl. Inst. and Meth. A 386 (1997) 531.
- [2] I. Giomataris, Ph. Rebourgeard, J.P. Robert, G. Charpak, Nucl. Inst. and Meth. A 376 (1996) 29.
- [3] F. Sauli, A. Sharma, Ann. Rev. Nucl. Part. Sci. 49(1999) 341.
- [4] C. Altunbas et al., Nucl. Inst. and Meth. A 490 (2002) 177.
- [5] <http://www.fair-center.eu/for-users/experiments/cbm.html> .
- [6] <http://www.fair-center.eu/> .
- [7] CBM Progress report, 2008.
- [8] S. Biswas et al., Nucl. Inst. and Meth. A 718 (2013) 403.
- [9] S. Biswas et al., Nucl. Inst. and Meth. A 800 (2015) 93.
- [10] S. Biswas et al., Nucl. Inst. and Meth. A 824 (2016) 504.
- [11] R. P. Adak et al., Nucl. Inst. and Meth. A846 (2017) 29. [arXiv:1604.02899v2].
- [12] S. Chatterjee et al., Nucl. Inst. and Meth. A 977 (2020) 164334.
- [13] S. Chatterjee et al., 2020 JINST 15 T09011 doi:10.1088/1748-0221/15/09/T09011.
- [14] ALICE Collaboration, ALICE-TDR-016, CERN-LHCC- 2013-020, March 3, 2014.
- [15] Saikat Biswas, (To be published in the Proceedings of 7th International Conference on Physics and Astrophysics of Quark Gluon Plasma), [arXiv:1511.04988].

- [16] Marco Villa et al., arXiv:1007.1131v1 [physics.ins-det] 7 Jul 2010.
- [17] GDD Group - CERN, <http://gdd.web.cern.ch/GDD/> .
- [18] <http://rd51-public.web.cern.ch/rd51-public/> .
- [19] V.N. Bychkov et al., Nucl. Inst. and Meth. A 556 (2006) 66-79.
- [20] <https://atlas.cern/discover/detector/inner-detector>
- [21] <https://home.cern/news/news/experiments/new-straw-trackers-na62>
- [22] Y. Van Haarlem et al., Nucl. Instr. and Meth. in Phys. A 622 (2019) 142.
- [23] C. Adorisio et al., Nucl. Inst. and Meth. A 575 (2007) 532.
- [24] T. Akesson et al., Nucl. Inst. and Meth. A 449 (2000) 446.
- [25] PANDA Collaboration, Technical Design Report for the: PANDA Straw Tube Tracker, [arXiv:1205.5441].
- [26] R. Santonico, R. Cardarelli, Nucl. Inst. and Meth. 187 (1981) 377.
- [27] Yu. N. Pestov, Nucl. Inst. and Meth. 196 (1982) 45.
- [28] W. B. Atwood et al., Nucl. Inst. and Meth. 206 (1983) 99.
- [29] M. Anelli et al., Nucl. Inst. and Meth. A 300 (1991) 572.
- [30] Gy. L. Bencze et al., Nucl. Inst. and Meth. A 340 (1994) 466.
- [31] R. Cardarelli et al., Nucl. Inst. and Meth. A 263 (1988) 20.
- [32] A. Blanco et al., Nucl. Inst. and Meth. A 513 (2003) 8.
- [33] A. Abashian et al., Nucl. Inst. and Meth. A 479 (2002) 117.
- [34] BaBar Technical Design Report, BaBar Collaboration, SLAC Report SLAC-R-95-457, March 1995.
- [35] The BESIII Detector, IHEP-BEPCII-SB-13, IHEP, Beijing.
- [36] ATLAS Technical Design Report, Muon Spectrometer, CERN/LHCC/97-22, Geneva, 1997.
- [37] CMS - Technical Proposal, CERN/LHCC/94-38, December 1994.
- [38] M. Guler et al., OPERA, an appearance experiment to search for ν_μ - ν_τ oscillations in the CNGS beam, CERN/SPSC 2000-028.
- [39] M. Couceiro et al., Nucl. Inst. and Meth. A 580 (2007) 915.
- [40] P. Camarri, Nucl. Inst. and Meth. A 572 (2007) 476.
- [41] M. Abbrescia et al., Nucl. Phys. B (Proc. Suppl.) 125 (2003) 43.
- [42] M. Abbrescia et al., Nucl. Inst. and Meth. A 506 (2003) 101.
- [43] P. Fonte et al., Nucl. Inst. and Meth. A 449 (2000) 295.
- [44] A. Blanco et al., Nucl. Inst. and Meth. A 535 (2004) 272.
- [45] S. Biswas et al., arXiv:0802.2766 [nucl-ex] 20 Feb 2008.
- [46] M.M. Aggarwal et al., Nucl. Inst. and Meth. A 499 (2003) 751.
- [47] M.M. Aggarwal et al., Nucl. Inst. and Meth. A 488 (2002) 131.
- [48] V.M. Datar et al., Nucl. Inst. and Meth. A 602 (2009) 744.
- [49] S. Biswas et al., Nucl. Inst. and Meth. A 602 (2009) 749.

- [50] S. Biswas et al., Nucl. Inst. and Meth. A 604 (2009) 310.
- [51] S. Biswas et al., Nucl. Inst. and Meth. A 617 (2010) 138.
- [52] S. Biswas et al., Nucl. Inst. and Meth. A 661 (2012) S94.
- [53] K.K. Meghna et al., 2012 JINST 7 P10003 doi:10.1088/1748-0221/7/10/P10003.
- [54] K.K. Meghna et al., Nucl. Inst. and Meth. A 816 (2016) 1.
- [55] A. Banerjee et al., Nucl. Inst. and Meth. A 718 (2013) 138.
- [56] R.P. Adak et al., 2016 JINST 11 T10001 doi:10.1088/1748-0221/11/10/T10001.
- [57] S. Roy et al., Nucl. Inst. and Meth. A 936 (2019) 485.
- [58] S. Chatterjee et al., Journal of Physics: Conference Series 1498 (2020) 012037.
- [59] S. Chatterjee et al., Nucl. Inst. and Meth. A 936 (2019) 491.
- [60] S. Roy et al., Nucl. Inst. and Meth. A 936 (2019) 488.
- [61] S. Chakraborty et al., Nucl. Inst. and Meth. A 936 (2019) 424.
- [62] A. Sen et al., 2020 JINST 15 C06055 doi:10.1088/1748-0221/15/06/C06055.
- [63] R. Patra et al., Nucl. Instrum. Meth. A 862 (2017) 25.
- [64] CDT CASCADE Detector Technologies GmbH, Hans-Bunte-Str. 8-10, 69123 Heidelberg, Germany, www.n-cdt.com.
- [65] S. Biswas et al., 2013 JINST 8 C12002 doi:10.1088/1748-0221/8/12/C12002.
- [66] R.N. Patra et al., Nucl. Inst. and Meth. A 824 (2016) 501.
- [67] S. Sahu et al., 2017 JINST 12 C05006 doi:10.1088/1748-0221/12/05/C05006.
- [68] S. Sahu et al., RD51-NOTE-2015-004, [arXiv:1507.03575v1].
- [69] F. Sauli, Principles of operation of multi wire proportional and drift chambers, CERN 77-09, 3 May 1977.
- [70] M.C. Altunbas et al., Nucl. Inst. and Meth. A 515 (2003) 249.
- [71] A. Orthen et al., Nucl. Inst. and Meth. A 512 (2003) 476.
- [72] A. Orthen et al., Nucl. Inst. and Meth. A 500 (2003) 163.
- [73] <http://cutecom.sourceforge.net/>
- [74] D. Nag et al., Advanced Detectors for Nuclear, High Energy and Astroparticle Physics, Springer Proceedings in Physics 201, <https://doi.org/10.1007/978-981-10-7665-7-21>.
- [75] K. K. Meghna et al., 2012 JINST 7 P10003 doi:10.1088/1748-0221/7/10/P10003.
- [76] E. Cerron Zeballos et al., Nucl. Inst. and Meth. A 374 (1996) 132.
- [77] W.J.Llope et al. Nucl. Inst. and Meth. A 661 (2012) S110-S113
- [78] R. Arnaldi et al., Nucl. Inst. and Meth. A 451 (2000) 462.
- [79] CMS Collaboration, Muon Project, CERN/LHCC 97-32.
- [80] D. Belver et al., Nucl. Inst. and Meth. A 602 (2009) 687.
- [81] J. Han et al., Nucl. Inst. and Meth. A 577 (2007) 552.
- [82] G. Aielli et al., Nucl. Inst. and Meth. A 562 (2006) 92.

- [83] R. Acquafredda et al., JINST 4 (2009) P04018.
- [84] Q. Zhang et al., Nucl. Inst. and Meth. A 583 (2007) 278.
- [85] I. Deppner et al., Nucl. Inst. and Meth. A 661 (2012) S121.
- [86] E. Nandy et al., Proceedings of the DAE-BRNS Symp. on Nucl. Phys. 61 (2016) 1024.
- [87] B. Liberti et al., Nuclear Physics B (Proc. Suppl.) 177178 (2008) 307.
- [88] A. Bergnoli et al., Nuclear Physics B (Proc. Suppl.) 158 (2006) 93.
- [89] A. Bergnoli et al., IEEE TRANSACTIONS ON NUCLEAR SCIENCE VOL. 52, NO. 6, DECEMBER 2005.
- [90] F. Bossu et al., JINST 7 (2012) T12002.